



High Order Asymptotic Preserving Hermite WENO Fast Sweeping Method for the Steady-State S_N Transport Equations

Yupeng Ren^{1,2} · Yulong Xing³ · Dean Wang⁴ · Jianxian Qiu⁵

Received: 17 September 2021 / Revised: 27 May 2022 / Accepted: 15 July 2022
© The Author(s), under exclusive licence to Springer Science+Business Media, LLC, part of Springer Nature 2022

Abstract

In this paper, we propose to combine the fifth-order Hermite weighted essentially non-oscillatory (HWENO) scheme and the fast sweeping method (FSM) for the solution of the steady-state S_N transport equation in the finite volume framework. It is well-known that the S_N transport equation asymptotically converges to a macroscopic diffusion equation in the limit of optically thick systems with small absorption and sources. Numerical methods which can preserve the asymptotic diffusion limit are referred to as asymptotic preserving methods. In the one-dimensional case, we provide the analysis to demonstrate the asymptotic preserving property of the high order finite volume HWENO method, by showing that its cell-edge and cell-average fluxes possess the thick diffusion limit. A hybrid strategy to compute the nonlinear weights in the HWENO reconstruction is introduced to save computational costs. Extensive one- and two-dimensional numerical experiments are performed to verify the accuracy, asymptotic preserving property and positivity of the proposed HWENO FSM. The proposed HWENO method can also be combined with the Diffusion Synthetic Acceleration algorithm to improve computational efficiency.

Keywords Weighted essentially non-oscillatory (WENO) method · Hermite method · Fast sweeping method · S_N transport equation · Asymptotic preserving property · Diffusion limit

1 Introduction

In this paper, we present a high order asymptotic preserving weighted essentially non-oscillatory (WENO) method for the steady-state transport equation, which can preserve the diffusion limit of the equation in the discrete setting. The radiative transport equation is a kinetic model which describes the scattering and absorbing of particles moving through a

The work of Y. Xing is partially supported by the NSF grant DMS-1753581.
The work of J. Qiu is partially supported by NSFC grant 12071392.

✉ Yulong Xing
xing.205@osu.edu

medium and plays an important role in a wide range of scientific and engineering applications. The steady-state monoenergetic linear transport equation takes the form

$$\Omega \cdot \nabla \psi(\mathbf{x}, \Omega) + \frac{\sigma_t}{\varepsilon} \psi(\mathbf{x}, \Omega) = \frac{1}{|\mathbb{S}^{d-1}|} \left(\left(\frac{\sigma_t}{\varepsilon} - \varepsilon \sigma_a \right) \phi(\mathbf{x}) + \varepsilon Q(\mathbf{x}) \right), \quad (\mathbf{x}, \Omega) \in D \times \mathbb{S}^{d-1}, \quad (1.1a)$$

$$\psi(\mathbf{x}, \Omega) = G(\mathbf{x}, \Omega), \quad (\mathbf{x}, \Omega) \in \Gamma^-, \quad (1.1b)$$

where $D \subseteq \mathbb{R}^d$ (with $d = 1, 2, 3$) is an open bounded domain. When $d = 3$, the set of propagation directions is the unit sphere \mathbb{S}^2 in \mathbb{R}^3 . When $d = 1, 2$, it becomes the projection of \mathbb{S}^2 onto \mathbb{R}^d , i.e., \mathbb{S}^1 is a unit disk if $d = 2$ and \mathbb{S}^0 is unit segment $[-1, 1]$ if $d = 1$. $\Gamma^- = \{(\mathbf{x}, \mathbf{v}) \in \partial D \times \mathbb{S}^{d-1} \mid \mathbf{n}(\mathbf{x}) \cdot \mathbf{v} < 0\}$ is the incoming boundary, with $\mathbf{n}(\mathbf{x})$ being the unit outer normal vector at $\mathbf{x} \in \partial D$. $\psi(\mathbf{x}, \Omega)$ denotes the angular intensity, and $\phi(\mathbf{x}) = \int_{\mathbb{S}^{d-1}} \psi d\Omega$ is the scalar flux representing the integral of ψ over \mathbb{S}^{d-1} . ε is the scaling parameter, representing the ratio of a particle mean free path to a characteristic scale length of the system. σ_t and σ_a are the non-dimensionalized total and absorption macroscopic cross section, respectively. The difference of them is the scattering macroscopic cross section, denoted by σ_s satisfying $\sigma_s = \sigma_t - \sigma_a$, which will be used later. $Q(\mathbf{x})$ is the external source function, and $G(\mathbf{x}, \Omega)$ is the given incoming flux on Γ^- .

It is well-known that when ε is very small uniformly in the entire domain, the angular flux ψ away from the boundary is nearly independent of the angular direction Ω , and the transport model can be accurately approximated by a macroscopic diffusion equation that depends on the variable \mathbf{x} only [13, 19, 22, 26, 32]. Asymptotic preserving (AP) numerical methods [16] refer to the methods that are accurate and robust in all regimes from transport dominated to diffusion dominated. AP discretization of the transport equation (1.1) reduces to a consistent and stable discretization of the macroscopic diffusion equation when ε goes to zero.

There have been extensive studies on various AP numerical methods for solving the linear transport equation. Larsen et al. first used asymptotic analysis to study the behavior of discrete transport solutions, and produced many important results on the relationship between the analytical and numerical solutions of the transport equations [1, 12, 20, 24, 25]. Larsen and others used the asymptotic expansion methods to analyze the behavior of several numerical schemes, such as the diamond difference method [9, 33], step difference method [9, 33], the Lund-Wilson method [29, 30] and Castor [10] method in the thick and intermediate regimes. Adams extended the asymptotic analysis to a complete family of discontinuous finite-element methods (DFEMs) and showed that some DFEM schemes do not possess the diffusion limit because the upwind numerical flux forces the scalar flux, and thus the angular flux, to be continuous across the mesh cells [1]. Guermond and Kanschat proved by using functional analytic tools that a necessary and sufficient condition for the standard upwind discontinuous Galerkin approximation to converge to the correct limit solution in the diffusive regime is that the approximation space contains a linear space of continuous functions, and the restrictions of the functions of this space to each mesh cell contain the linear polynomials [12]. Most recently, Wang has derived a theoretical result to determine the mesh size for a variety of finite difference schemes to achieve accurate results in the diffusion limit [43].

The finite volume Hermite WENO (HWENO) method will be considered in this paper. WENO methods are a class of high order numerical methods for solving the hyperbolic conservation laws, which yield very robust and non-oscillatory solutions near the shocks, and have been widely used in applications. Recently, high order HWENO methods, with a more compact reconstruction stencil, have also gained much attention in solving hyperbolic

conservation laws. The HWENO and WENO methods have similar building blocks, and the major difference between them is that the HWENO method uses both the unknown function and its first derivative (or first moment) in the reconstruction and update procedure. The HWENO scheme was first proposed as a robust limiter for the discontinuous Galerkin (DG) method in [35, 36], thanks to the compact stencil required in its reconstruction steps. In [37, 54], the HWENO scheme was extended to solve the Hamilton-Jacobi equations, and achieved very good numerical results. Compared with the standard WENO scheme, its boundary treatment is much simpler and the numerical error is observed to be smaller with the same meshes, as shown in [37]. The HWENO scheme was later extended to solve the hyperbolic conservation laws in the finite difference [28] and finite volume [53] frameworks, and the same advantages have been observed.

In the past few decades, many efficient numerical solvers for the static hyperbolic conservation laws and Hamilton-Jacobi equations have been developed. Among them, one of the most popular methods is the fast sweeping method (FSM) [17, 34, 41, 52], which was first proposed by Boué and Dupuis [4] to solve a deterministic control problem with quadratic running cost using Markov chain approximation. In [52], a systematic way for solving the Eikonal equations using FSM was introduced by Zhao. Later, many high order FSMs have been developed to solve static Hamilton-Jacobi equations, in the framework of finite difference WENO [14, 48, 51] and finite element DG [27, 31, 46, 49] methods. In [8], high order WENO FSM was proposed for solving the steady-state hyperbolic conservation laws with source terms. In [7] and [47], FSM was combined with the fixed point iteration idea, first proposed in [50], to provide an efficient WENO solver for the steady-state hyperbolic conservation laws. In this paper, we propose to combine the finite volume HWENO method with the fast sweeping technique, and apply them to the steady-state linear transport equations. In the angular discretization, we adopt the discrete ordinate (S_N) method, in which the angular variable is discretized into a finite number of directions, see [23] and the references therein for more discussions on the S_N method. The main novel contribution of this paper is to present a class of high order AP methods, by demonstrating that the proposed finite volume HWENO FSM preserves the asymptotic diffusion limit when $\varepsilon \rightarrow 0$. Many high order AP methods have been studied for the linear transport equations in the literature, and most of their spatial discretizations are in the DG framework. While DG methods enjoy many advantages including their robustness, flexibility and AP property (under certain conditions on the polynomial spaces, see [1, 12]), they are also known to be computationally expensive in multi dimensions when the polynomial degree becomes large. In [43], it was shown that the original WENO method does not have the AP property. We also investigated finite difference HWENO FSM and numerical results indicate that it is not AP. Here we present a high order finite volume HWENO method (fifth-order HWENO is presented as an example, although the same idea can be extended to higher order if needed), which can be proven to have the AP property following the similar approach in [24] to show the AP property of the linear discontinuous (LD) method. The proposed method can also be viewed as the higher-order extension of the LD method in one dimension, and that of the bilinear discontinuous finite element method [6] in multi dimensions. In addition, we present a hybrid strategy to reduce the computational cost of evaluating the nonlinear weights in the HWENO reconstruction, which was shown to save about 50% CPU time in the numerical tests. In the two-dimensional case, we employ the dimension-by-dimension HWENO reconstruction procedure in the finite volume framework as in [54], which can achieve the same essentially non-oscillatory property as the genuine two-dimensional strategy, and is easier to code than the latter one. Both one- and two-dimensional algorithms have been studied, and extensive numerical examples are provided to confirm the AP property and robustness of the proposed methods. Finally,

we will combine the HWENO method and diffusion synthetic acceleration (DSA) method [3, 5, 18, 21, 38] to improve the computational efficiency, and present a numerical example on the fixed-source neutron transport equation with different scattering ratios to illustrate the acceleration via DSA.

The rest of the paper is organized as follows. In Sect. 2, we describe in detail the HWENO FSM for S_N transport equation in one-dimensional (1D) case. The analysis of thick diffusion limit is also provided. In the Sect. 3, we introduce the HWENO FSM for the multidimensional S_N transport equation, and provide the flowchart of HWENO FSM in the two-dimensional (2D) setting. The numerical examples are performed to demonstrate the high accuracy, positive and thick diffusion limit of our proposed schemes in Sect. 4. In Sect. 5, the acceleration of HWENO method via DSA is investigated. Some conclusion remarks are presented in Sect. 6.

2 One-Dimensional S_N Transport Equation

In this section, we will present the HWENO FSM for the 1D transport equation in the finite volume framework, and analyze the diffusion limit of the resulting method.

2.1 Mathematical Model and HWENO Method

The steady-state, monoenergetic, discrete ordinates S_N transport equation in 1D slab geometry $[0, L]$ with isotropic scattering takes the form [25]

$$\mu_m \frac{d}{dx} \psi(x, \mu_m) + \frac{\sigma_t}{\varepsilon} \psi(x, \mu_m) = \frac{1}{2} \left(\frac{\sigma_t}{\varepsilon} - \varepsilon \sigma_a \right) \sum_{m=1}^M \psi(x, \mu_m) \omega_m + \frac{\varepsilon}{2} Q(x), \quad 1 \leq m \leq M, \tag{2.1a}$$

$$\psi(0, \mu_m) = f(\mu_m) = f_m, \quad 0 < \mu_m \leq 1, \tag{2.1b}$$

$$\psi(L, \mu_m) = g(\mu_m) = g_m, \quad -1 \leq \mu_m < 0, \tag{2.1c}$$

where $\sum_{m=1}^M \psi(x, \mu_m) \omega_m := \phi(x)$ is the scalar flux, with ω_m being the Gaussian quadrature weights. M is assumed to be an even integer in this paper, which means a symmetric quadrature set is used. The symmetric quadrature set $\{\mu_m, \omega_m\}$ satisfies

$$\sum_{m=1}^M (\mu_m)^k \omega_m = \begin{cases} 2, & k = 0, \\ 0, & \text{for } k \text{ odd,} \\ \frac{2}{k+1}, & \text{for } k \text{ even,} \end{cases} \tag{2.2}$$

where k is an integer with $k \leq 2M - 1$.

We assume the computational domain $[0, L]$ has been divided into cells $I_j = [x_{j-\frac{1}{2}}, x_{j+\frac{1}{2}}]$, $j = 1, \dots, J$ for all m . The cell center and the mesh size are denoted as $x_j = (x_{j-\frac{1}{2}} + x_{j+\frac{1}{2}})/2$ and $\Delta x_j = x_{j+\frac{1}{2}} - x_{j-\frac{1}{2}}$ as in Fig. 1. Let $\psi_m(x) = \psi(x, \mu_m)$, we define

$$\psi_{m,j} = \frac{1}{\Delta x_j} \int_{I_j} \psi_m(x) dx, \quad \widehat{\psi}_{m,j} = \frac{1}{\Delta x_j} \int_{I_j} \psi_m(x) \frac{x - x_j}{\Delta x_j} dx, \tag{2.3}$$

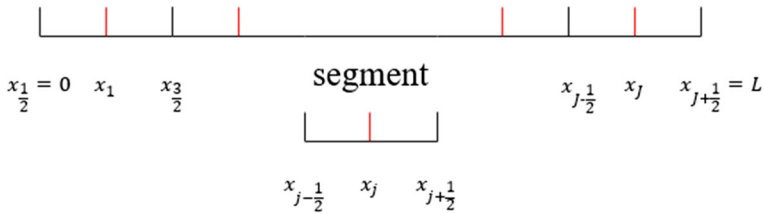


Fig. 1 The segment in one-dimensional case

as the numerical approximation to the average of angular flux and its first moment. Similarly, we can define

$$\begin{aligned}
 Q_j &= \frac{1}{\Delta x_j} \int_{I_j} Q(x) dx, \quad \widehat{Q}_j = \frac{1}{\Delta x_j} \int_{I_j} Q(x) \frac{x - x_j}{\Delta x_j} dx; \\
 \phi_j &= \frac{1}{\Delta x_j} \int_{I_j} \phi(x) dx = \frac{1}{\Delta x_j} \int_{I_j} \sum_{m=1}^M \psi(x, \mu_m) \omega_m dx = \sum_{m=1}^M \psi_{m,j} \omega_m; \tag{2.4}
 \end{aligned}$$

$$\widehat{\phi}_j = \frac{1}{\Delta x_j} \int_{I_j} \phi(x) \frac{x - x_j}{\Delta x_j} dx = \frac{1}{\Delta x_j} \int_{I_j} \sum_{m=1}^M \psi(x, \mu_m) \omega_m \frac{x - x_j}{\Delta x_j} dx = \sum_{m=1}^M \widehat{\psi}_{m,j} \omega_m. \tag{2.5}$$

We assume that material properties σ_t, σ_a are constants within each cell but can vary between cells, which means that cell-wise constant cross sections will be considered. This assumption has been adopted in many studies on neutron transport equations [1, 24, 25]. Multiplying (2.1) by $\frac{1}{\Delta x_j}$ and $\frac{x - x_j}{\Delta x_j}$ respectively, integrating on cell I_j and applying integration by parts yield

$$\frac{1}{\Delta x_j} \int_{I_j} (\mu_m \psi_m(x))_x dx + \frac{\sigma_{t,j}}{\varepsilon} \psi_{m,j} = \frac{1}{2} \left(\frac{\sigma_{t,j}}{\varepsilon} - \varepsilon \sigma_{a,j} \right) \sum_{k=1}^M \psi_{k,j} \omega_k + \frac{\varepsilon}{2} Q_j, \tag{2.6a}$$

$$\begin{aligned}
 &\frac{1}{\Delta x_j} \left(\frac{1}{2} (\mu_m \psi_{m,j+\frac{1}{2}} + \mu_m \psi_{m,j-\frac{1}{2}}) - \mu_m \psi_{m,j} \right) + \frac{\sigma_{t,j}}{\varepsilon} \widehat{\psi}_{m,j} \\
 &= \frac{1}{2} \left(\frac{\sigma_{t,j}}{\varepsilon} - \varepsilon \sigma_{a,j} \right) \sum_{k=1}^M \widehat{\psi}_{k,j} \omega_k + \frac{\varepsilon}{2} \widehat{Q}_j, \tag{2.6b}
 \end{aligned}$$

$$\psi(0, \mu_m) = f_m, \quad 0 < \mu_m \leq 1, \tag{2.6c}$$

$$\psi(L, \mu_m) = g_m, \quad -1 \leq \mu_m < 0, \tag{2.6d}$$

where the following equality with $F_m(\psi) = \mu_m \psi_m(x)$

$$\int_{I_j} (F_m(\psi))_x \frac{x - x_j}{\Delta x_j} dx = \frac{1}{2} \left(F_m(x_{j+\frac{1}{2}}^-) + F_m(x_{j-\frac{1}{2}}^+) \right) - \mu_m \psi_{m,j} \tag{2.7}$$

is used in the derivation of the second equation.

The HWENO numerical discretizations of Eq. (2.1) are now given by

$$\begin{aligned} \frac{1}{\Delta x_j} \left(\widehat{F}_{m,j+\frac{1}{2}} - \widehat{F}_{m,j-\frac{1}{2}} \right) + \frac{\sigma_{t,j}}{\varepsilon} \psi_{m,j} &= \frac{1}{2} \left(\frac{\sigma_{t,j}}{\varepsilon} - \varepsilon \sigma_{a,j} \right) \sum_{k=1}^M \psi_{k,j} \omega_k \\ &+ \frac{\varepsilon}{2} Q_j, \\ \frac{1}{\Delta x_j} \left(\frac{1}{2} (\widehat{F}_{m,j+\frac{1}{2}} + \widehat{F}_{m,j-\frac{1}{2}}) - \mu_m \psi_{m,j} \right) + \frac{\sigma_{t,j}}{\varepsilon} \widehat{\psi}_{m,j} &= \frac{1}{2} \left(\frac{\sigma_{t,j}}{\varepsilon} - \varepsilon \sigma_{a,j} \right) \sum_{k=1}^M \widehat{\psi}_{k,j} \omega_k \\ &+ \frac{\varepsilon}{2} \widehat{Q}_j, \end{aligned} \tag{2.8}$$

with $\widehat{F}_{m,j\pm\frac{1}{2}}$ being the numerical fluxes to be specified, and $\psi_{m,\frac{1}{2}} = f_m$ if $\mu_m > 0$ and $\psi_{m,J+\frac{1}{2}} = g_m$ if $\mu_m < 0$. In this paper, we use the Godunov numerical flux [11], taking the form

$$\widehat{F}_{m,j+\frac{1}{2}} = \begin{cases} \min_{\psi_{m,j+\frac{1}{2}}^- \leq \psi \leq \psi_{m,j+\frac{1}{2}}^+} \mu_m \psi_m, & \text{if } \psi_{m,j+\frac{1}{2}}^- \leq \psi_{m,j+\frac{1}{2}}^+; \\ \max_{\psi_{m,j+\frac{1}{2}}^+ \leq \psi \leq \psi_{m,j+\frac{1}{2}}^-} \mu_m \psi_m, & \text{if } \psi_{m,j+\frac{1}{2}}^- > \psi_{m,j+\frac{1}{2}}^+. \end{cases} \tag{2.9}$$

The Godunov flux can be further simplified for our linear flux, which leads to the following two cases:

- If $\mu_m > 0$, the HWENO scheme (2.8) becomes

$$\begin{aligned} \frac{\mu_m}{\Delta x_j} \left(\psi_{m,j+\frac{1}{2}}^- - \psi_{m,j-\frac{1}{2}}^- \right) + \frac{\sigma_{t,j}}{\varepsilon} \psi_{m,j} &= \frac{1}{2} \left(\frac{\sigma_{t,j}}{\varepsilon} - \varepsilon \sigma_{a,j} \right) \sum_{k=1}^M \psi_{k,j} \omega_k \\ &+ \frac{\varepsilon}{2} Q_j, \\ \frac{\mu_m}{\Delta x_j} \left(\frac{1}{2} (\psi_{m,j+\frac{1}{2}}^- + \psi_{m,j-\frac{1}{2}}^-) - \psi_{m,j} \right) + \frac{\sigma_{t,j}}{\varepsilon} \widehat{\psi}_{m,j} &= \frac{1}{2} \left(\frac{\sigma_{t,j}}{\varepsilon} - \varepsilon \sigma_{a,j} \right) \sum_{k=1}^M \widehat{\psi}_{k,j} \omega_k \\ &+ \frac{\varepsilon}{2} \widehat{Q}_j, \end{aligned} \tag{2.10}$$

with $\psi_{m,\frac{1}{2}} = f_m$.

- If $\mu_m < 0$, the HWENO scheme (2.8) becomes

$$\begin{aligned} \frac{\mu_m}{\Delta x_j} \left(\psi_{m,j+\frac{1}{2}}^+ - \psi_{m,j-\frac{1}{2}}^+ \right) + \frac{\sigma_{t,j}}{\varepsilon} \psi_{m,j} &= \frac{1}{2} \left(\frac{\sigma_{t,j}}{\varepsilon} - \varepsilon \sigma_{a,j} \right) \sum_{k=1}^M \psi_{k,j} \omega_k \\ &+ \frac{\varepsilon}{2} Q_j, \\ \frac{\mu_m}{\Delta x_j} \left(\frac{1}{2} (\psi_{m,j+\frac{1}{2}}^+ + \psi_{m,j-\frac{1}{2}}^+) - \psi_{m,j} \right) + \frac{\sigma_{t,j}}{\varepsilon} \widehat{\psi}_{m,j} &= \frac{1}{2} \left(\frac{\sigma_{t,j}}{\varepsilon} - \varepsilon \sigma_{a,j} \right) \sum_{k=1}^M \widehat{\psi}_{k,j} \omega_k \\ &+ \frac{\varepsilon}{2} \widehat{Q}_j, \end{aligned} \tag{2.11}$$

with $\psi_{m,J+\frac{1}{2}} = g_m$.

Remark 2.1 For the problems with spatially varying cross sections, examples of simulations that may not be adequately described by cell-wise constant cross sections include nuclear reactor depletion calculations and radiative transfer calculations for high energy density physics experiments. The accuracy of the finite volume HWENO method studied here may be affected due to the approximate coefficients $\sigma_{t,j}$ and $\sigma_{a,j}$ in the j th cell. The HWENO method can also be extended to solve such problems with high order accuracy, but the corresponding iterative scheme is no longer the same as numerical quadrature rule and Newton iteration will be introduced, and the asymptotic analysis will be different.

Next, we will present the HWENO reconstruction procedure to evaluate the high-order interface value approximations $\psi_{m,j \pm \frac{1}{2}}^\mp$ from the cell average values $\psi_{m,j}$ and the first moments $\widehat{\psi}_{m,j}$. For ease of presentation, we assume the mesh is uniform, i.e. $\Delta x_j = \Delta x$ for all j . The detailed procedure of the HWENO reconstruction is summarized as follows:

1. Based on three small stencils $\mathbb{S}_0 = \{I_{j-1}, I_j\}$, $\mathbb{S}_1 = \{I_j, I_{j+1}\}$, $\mathbb{S}_2 = \{I_{j-1}, I_j, I_{j+1}\}$, and their union $\mathbb{T} = \{\mathbb{S}_0, \mathbb{S}_1, \mathbb{S}_2\}$, we construct three Hermite cubic polynomials $p_0(x)$, $p_1(x)$, $p_2(x)$, and a fifth-order polynomial $q(x)$ such that

$$\begin{aligned} \frac{1}{\Delta x} \int_{I_{j+i}} p_0(x) dx &= \psi_{m,j+i}, & \frac{1}{\Delta x} \int_{I_{j+i}} p_0(x) \frac{x - x_{j+i}}{\Delta x} dx &= \widehat{\psi}_{m,j+i}, & i &= -1, 0, \\ \frac{1}{\Delta x} \int_{I_{j+i}} p_1(x) dx &= \psi_{m,j+i}, & \frac{1}{\Delta x} \int_{I_{j+i}} p_1(x) \frac{x - x_{j+i}}{\Delta x} dx &= \widehat{\psi}_{m,j+i}, & i &= 0, 1, \\ \frac{1}{\Delta x} \int_{I_{j+i}} p_2(x) dx &= \psi_{m,j+i}, & \frac{1}{\Delta x} \int_{I_j} p_2(x) \frac{x - x_j}{\Delta x} dx &= \widehat{\psi}_{m,j}, & i &= -1, 0, 1, \\ \frac{1}{\Delta x} \int_{I_{j+i}} q(x) dx &= \psi_{m,j+i}, & \frac{1}{\Delta x} \int_{I_{j+i}} q(x) \frac{x - x_{j+i}}{\Delta x} dx &= \widehat{\psi}_{m,j+i}, & i &= -1, 0, 1. \end{aligned}$$

Only the values of these polynomials at the cell interfaces $x = x_{j \pm \frac{1}{2}}$ are needed, and they take the form

$$p_0(x_{j-\frac{1}{2}}^+) = \frac{1}{2} \psi_{m,j-1} + \frac{1}{2} \psi_{m,j} + 2\widehat{\psi}_{m,j-1} - 2\widehat{\psi}_{m,j}; \tag{2.12a}$$

$$p_0(x_{j+\frac{1}{2}}^-) = \frac{3}{4} \psi_{m,j-1} + \frac{1}{4} \psi_{m,j} + \frac{7}{2} \widehat{\psi}_{m,j-1} + \frac{23}{2} \widehat{\psi}_{m,j}; \tag{2.12b}$$

$$p_1(x_{j-\frac{1}{2}}^+) = \frac{1}{4} \psi_{m,j} + \frac{3}{4} \psi_{m,j+1} - \frac{23}{2} \widehat{\psi}_{m,j} - \frac{7}{2} \widehat{\psi}_{m,j+1}; \tag{2.12c}$$

$$p_1(x_{j+\frac{1}{2}}^-) = \frac{1}{2} \psi_{m,j} + \frac{1}{2} \psi_{m,j+1} + 2\widehat{\psi}_{m,j} - 2\widehat{\psi}_{m,j+1}; \tag{2.12d}$$

$$p_2(x_{j-\frac{1}{2}}^+) = \frac{7}{66} \psi_{m,j-1} + \frac{5}{6} \psi_{m,j} + \frac{2}{33} \psi_{m,j+1} - \frac{60}{11} \widehat{\psi}_{m,j}; \tag{2.12e}$$

$$p_2(x_{j+\frac{1}{2}}^-) = \frac{2}{33} \psi_{m,j-1} + \frac{5}{6} \psi_{m,j} + \frac{7}{66} \psi_{m,j+1} + \frac{60}{11} \widehat{\psi}_{m,j}; \tag{2.12f}$$

$$q(x_{j-\frac{1}{2}}^+) = \frac{8}{27} \psi_{m,j-1} + \frac{7}{12} \psi_{m,j} + \frac{13}{108} \psi_{m,j+1} + \frac{28}{27} \widehat{\psi}_{m,j-1} - \frac{241}{54} \widehat{\psi}_{m,j} - \frac{25}{54} \widehat{\psi}_{m,j+1}; \tag{2.12g}$$

$$q(x_{j+\frac{1}{2}}^-) = \frac{13}{108} \psi_{m,j-1} + \frac{7}{12} \psi_{m,j} + \frac{8}{27} \psi_{m,j+1} + \frac{25}{54} \widehat{\psi}_{m,j-1} + \frac{241}{54} \widehat{\psi}_{m,j} - \frac{28}{27} \widehat{\psi}_{m,j+1}; \tag{2.12h}$$

2. For each small stencil $S_k, k = 0, 1, 2$, we compute the smooth indicators respectively, which measure the smoothness of the reconstructed polynomials $p_k(x), k = 0, 1, 2$, in the target cell I_j . The smaller the indicator is, the smoother the polynomial is in the target cells. Generally speaking, the smooth indicators are defined as [15]

$$\beta_k = \sum_{l=1}^3 \int_{I_j} \Delta x^{2l-1} \left(\frac{\partial^l}{\partial x^l} p_k(x) \right)^2 dx, \quad k = 0, 1, 2, \tag{2.13}$$

and their specific expressions are given by

$$\begin{aligned} \beta_0 &= \frac{1}{16} (\psi_{m,j} - \psi_{m,j-1} - 54\widehat{\psi}_{m,j} - 6\widehat{\psi}_{m,j-1})^2 \\ &\quad + \frac{39}{16} (-5\psi_{m,j-1} + 5\psi_{m,j} - 38\widehat{\psi}_{m,j} - 22\widehat{\psi}_{m,j-1})^2 \\ &\quad + \frac{3905}{16} (-\psi_{m,j-1} + \psi_{m,j} - 6\widehat{\psi}_{m,j} - 6\widehat{\psi}_{m,j-1})^2, \\ \beta_1 &= \frac{1}{16} (\psi_{m,j} - \psi_{m,j+1} + 54\widehat{\psi}_{m,j} + 6\widehat{\psi}_{m,j+1})^2 \\ &\quad + \frac{39}{16} (-5\psi_{m,j+1} + 5\psi_{m,j} + 38\widehat{\psi}_{m,j} + 22\widehat{\psi}_{m,j+1})^2 \\ &\quad + \frac{3905}{16} (-\psi_{m,j+1} + \psi_{m,j} + 6\widehat{\psi}_{m,j} + 6\widehat{\psi}_{m,j+1})^2, \\ \beta_2 &= \frac{1}{484} (-\psi_{m,j-1} + \psi_{m,j+1} + 240\widehat{\psi}_{m,j})^2 + \frac{13}{12} (-\psi_{m,j-1} + 2\psi_{m,j} - \psi_{m,j+1})^2 \\ &\quad + \frac{355}{44} (-\psi_{m,j+1} + \psi_{m,j-1} + 24\widehat{\psi}_{m,j})^2. \end{aligned}$$

In this paper, we follow the approach in [45], and use $\beta'_k = \tau_k \beta_k, k = 1, 2, 3$ as the smoothness indicator, where

$$\begin{aligned} \tau_0 &= \max [|\sigma_{t,j+1} - \sigma_{t,j}|, |\sigma_{s,j+1} - \sigma_{s,j}|] \Delta x, \\ \tau_1 &= \max [|\sigma_{t,j} - \sigma_{t,j-1}|, |\sigma_{s,j} - \sigma_{s,j-1}|] \Delta x \end{aligned}$$

and $\tau_2 = \max[\tau_0, \tau_1]$. These parameters are introduced in [45] to estimate the local material heterogeneity, and for the steady-state linear problem studied in this paper, it is known that the discontinuity will appear only at the location when the heterogeneity occurs.

3. We compute the linear weights, denoted by $\gamma_k(x_{j\pm\frac{1}{2}}^\mp), k = 0, 1, 2$, satisfying

$$q(x_{j\pm\frac{1}{2}}^\mp) = \sum_{k=0}^2 \gamma_k(x_{j\pm\frac{1}{2}}^\mp) p_k(x_{j\pm\frac{1}{2}}^\mp) \tag{2.14}$$

in the smooth regions, which leads to the values

$$\begin{aligned} \gamma_0(x_{j-\frac{1}{2}}^+) &= \frac{14}{27}, \quad \gamma_1(x_{j-\frac{1}{2}}^+) = \frac{25}{189}, \quad \gamma_2(x_{j-\frac{1}{2}}^+) = \frac{22}{63}, \\ \gamma_0(x_{j+\frac{1}{2}}^-) &= \frac{25}{189}, \quad \gamma_1(x_{j+\frac{1}{2}}^-) = \frac{14}{27}, \quad \gamma_2(x_{j+\frac{1}{2}}^-) = \frac{22}{63}. \end{aligned}$$

4. To eliminate the possible oscillation during the reconstruction procedure, we combine the linear weights and smoothness indicators to evaluate the nonlinear weights [15]

$$\bar{\omega}_k(x_{j\pm\frac{1}{2}}^\mp) = \frac{\tilde{\omega}_k(x_{j\pm\frac{1}{2}}^\mp)}{\sum_\ell \tilde{\omega}_\ell(x_{j\pm\frac{1}{2}}^\mp)}, \quad \tilde{\omega}_k(x_{j\pm\frac{1}{2}}^\mp) = \frac{\gamma_k(x_{j\pm\frac{1}{2}}^\mp)}{(\beta'_k + \tilde{\varepsilon})^2}, \quad k = 0, 1, 2, \quad (2.15)$$

where $\tilde{\varepsilon}$ is a small positive number to avoid the denominator becoming zero, and is taken as $\tilde{\varepsilon} = 10^{-6}$. The actual HWENO approximations of the cell interface values take the form

$$\psi_{m,j\pm\frac{1}{2}}^\mp = \sum_{k=0}^2 \bar{\omega}_k(x_{j\pm\frac{1}{2}}^\mp) p_k(x_{j\pm\frac{1}{2}}^\mp), \quad (2.16)$$

with $p_k(x_{j\pm\frac{1}{2}}^\mp)$ defined in (2.12a)–(2.12f).

Remark 2.2 It is not difficult to observe from (2.13) that, if both σ_t and σ_s are constants in the big stencil \mathbb{T} , the corresponding β'_m equals to zero. Therefore, we can replace the nonlinear HWENO reconstruction (2.16) by the following linear approximation in (2.12g)–(2.12h)

$$\psi_{m,j-\frac{1}{2}}^+ = \frac{8}{27}\psi_{m,j-1} + \frac{7}{12}\psi_{m,j} + \frac{13}{108}\psi_{m,j+1} + \frac{28}{27}\hat{\psi}_{m,j-1} - \frac{241}{54}\hat{\psi}_{m,j} - \frac{25}{54}\hat{\psi}_{m,j+1}; \quad (2.17a)$$

$$\psi_{m,j+\frac{1}{2}}^- = \frac{13}{108}\psi_{m,j-1} + \frac{7}{12}\psi_{m,j} + \frac{8}{27}\psi_{m,j+1} + \frac{25}{54}\hat{\psi}_{m,j-1} + \frac{241}{54}\hat{\psi}_{m,j} - \frac{28}{27}\hat{\psi}_{m,j+1}. \quad (2.17b)$$

This hybrid strategy is valid since the shock will not appear for this steady-state linear equation in the region when σ_t and σ_s are both constants. From the numerical results in Sect. 4, it can be observed that this strategy can save about 50% CPU time.

2.2 Fast Sweeping Idea to Solve the Global Linear System

The proposed HWENO scheme for the linear transport equation takes the form of (2.10) or (2.11), combined with the HWENO reconstruction of $\psi_{m,j\pm\frac{1}{2}}^\mp$. This is a large system involving the flux term (coupling in x direction) on the left side and the summation term (coupling in Ω direction) on the right side. The fast sweeping idea is adopted to solve this system efficiently. Let us first denote the right-hand side term of the two equations in (2.10) as S_j and \hat{S}_j , respectively. We summarize the flowchart of HWENO FSM for S_N equation in 1D as follows and refer to [51, 52] for more details of the FSM.

Step 1. Initialization: We take 0 as the initial guess of the unknowns $\psi_{m,j}$ and $\hat{\psi}_{m,j}$ for all m and j , and evaluate S_j and \hat{S}_j .

Step 2. Gauss-Seidel iteration with alternating sweeps. We sweep the whole domain with the following two alternating orderings repeatedly for each m :

(I) $j = 1 \rightarrow J$: if $\mu_m > 0$, solve the system (2.10) for each j from left to right. After updating the approximation $\psi_{m,j}$ and $\hat{\psi}_{m,j}$ in the cell I_j , we can apply HWENO reconstruction to obtain the cell-edge flux $\psi_{m,j+\frac{1}{2}}^-$ based on the most updated values of $\psi_{m,j+i}$ and $\hat{\psi}_{m,j+i}$ ($i = -1, 0, 1$).

(II) $j = J \rightarrow 1$: if $\mu_m < 0$, solve the system (2.11) for each j from right to left. After updating the approximation $\psi_{m,j}$ and $\hat{\psi}_{m,j}$ in the cell I_j , we can apply HWENO

reconstruction to obtain the cell-edge flux $\psi_{m,j-\frac{1}{2}}^+$ based on the most updated values of $\psi_{m,j+i}$ and $\widehat{\psi}_{m,j+i}$ ($i = -1, 0, 1$).

At the boundary of the computational domain, high-order extrapolations are used to compute the values at the ghost cells, which are needed for the HWENO reconstruction near the boundary. After repeating this process for all m directions, we can compute scalar flux ϕ_j , $\widehat{\phi}_j$ from $\psi_{m,j}$, $\widehat{\psi}_{m,j}$ via Gauss quadrature (2.4)–(2.5), and update S_j , \widehat{S}_j . This completes one Gauss-Seidel iteration.

Step 3. Convergence: Repeat the Gauss-Seidel iteration until the convergence criteria is satisfied. In this paper, if the scalar flux satisfies

$$\delta = \|\phi^{new} - \phi^{old}\|_{L_1} < 10^{-14},$$

for two consecutive iteration steps, we stop the iteration.

The pseudo code of **Step 2** is presented in Algorithm 1, where the superscript n indicates the results in “ n -th” iteration.

Algorithm 1 The Gauss-Seidel iteration of evaluating the scalar flux ψ^{n+1} from ψ^n

Require: The values of $\psi_{m,j}$, S_j and \widehat{S}_j after n -th iteration.

for $m = 1$ **to** M **do**

if $\mu_m > 0$ **then**

$\psi_{m,\frac{1}{2}} \leftarrow f_m$

for $j = 1$ **to** J **do**

 Solve (2.10) to obtain $\psi_{m,j}$ and $\widehat{\psi}_{m,j}$

 Compute cell-edge $\psi_{m,j+\frac{1}{2}} = \psi_{m,j+\frac{1}{2}}^-$ by HWENO reconstruction

end for

 High order extrapolation are used to compute the values at the ghost cells

else

$\psi_{m,J+\frac{1}{2}} \leftarrow g_m$

for $j = J$ **to** 1 **do**

 Solve (2.11) to obtain $\psi_{m,j}$ and $\widehat{\psi}_{m,j}$

 Compute cell-edge $\psi_{m,j-\frac{1}{2}} = \psi_{m,j-\frac{1}{2}}^+$ by HWENO reconstruction

end for

 High order extrapolation are used to compute the values at the ghost cells

end if

end for

for $j = 1$ **to** J **do**

$$\phi_j = \sum_{m=1}^M \psi_{m,j} \omega_m, \quad \widehat{\phi}_j = \sum_{m=1}^M \widehat{\psi}_{m,j} \omega_m$$

$$S_j = \frac{1}{2} \left(\frac{\sigma_{t,j}}{\varepsilon} - \varepsilon \sigma_{a,j} \right) \phi_j + \frac{\varepsilon}{2} Q_j, \quad \widehat{S}_j = \frac{1}{2} \left(\frac{\sigma_{t,j}}{\varepsilon} - \varepsilon \sigma_{a,j} \right) \widehat{\phi}_j + \frac{\varepsilon}{2} \widehat{Q}_j$$

end for

if $\delta = \|\phi^{n+1} - \phi^n\|_{L_1} < 10^{-14}$ **then**

 Stop iterate

else

 Return to the top and continue the iteration

end if

Remark 2.3 The high-order extrapolations are used to evaluate the values at the ghost cells. Because the stencil of HWENO method is more compact than that of WENO method, we need only one ghost cell in the left and right boundaries of the computational domain, respectively.

Remark 2.4 Note that the alternating sweeping direction described here is different from that in [51, 52]. If the characteristic direction is unknown, the sweeping direction was from left to right and then from right to left for one-dimensional problems. Here, since the neutron characteristics direction is available, namely from left to right when $\mu_m > 0$ and from right to left when $\mu_m < 0$, we set the sweeping direction in the same way, which has also been utilized in [45].

2.3 Thick Diffusion Limit

One focus of the proposed HWENO method is its AP property when ε is small. In this subsection, we will provide the mathematical analysis to study the thick diffusion limit of the HWENO method. It will be shown that the cell-edge and cell-average fluxes possess a thick diffusion limit, and the HWENO method is very accurate for problems with anisotropic boundary fluxes. The detailed analysis is inspired by that of the LD method in [24].

It is known that when $\varepsilon \rightarrow 0$, the solution of the 1D linear transport equation (2.1) satisfies [24, 25]

$$\psi(x, \mu) = \frac{\phi(x)}{2} + O(\varepsilon), \tag{2.18}$$

where $\phi(x)$ is the solution of the diffusion equation

$$-\frac{d}{dx} \frac{1}{3\sigma_t} \frac{d}{dx} \phi + \sigma_a \phi = Q, \tag{2.19}$$

with appropriate boundary conditions, and we refer to [24] for more discussions on this.

Below, we will analyze the asymptotic diffusion limit of the HWENO FSM with linear reconstruction, and verify that it is a consistent approximation of the diffusion equation (2.19). We start by presenting the HWENO method in the asymptotic form, plugging in the suitable ansatz, and collecting the equations with different orders of ε . Since the proof is lengthy, the detailed proof of the AP property is separated into four steps summarized as follows.

Let us rewrite the HWENO FSM (2.10)–(2.11) in the following asymptotic form

$$\begin{aligned} \frac{\mu_m}{\Delta x_j} \left(\psi_{m,j+\frac{1}{2}} - \psi_{m,j-\frac{1}{2}} \right) + \frac{\sigma_{t,j}}{\varepsilon} \psi_{m,j} &= \frac{1}{2} \left(\frac{\sigma_{t,j}}{\varepsilon} - \varepsilon \sigma_{a,j} \right) \sum_{k=1}^M \psi_k \omega_k \\ &\quad + \frac{\varepsilon Q_j}{2}, \\ \frac{\mu_m}{\Delta x_j} \left(\frac{1}{2} (\psi_{m,j+\frac{1}{2}} + \psi_{m,j-\frac{1}{2}}) - \psi_{m,j} \right) + \frac{\sigma_{t,j}}{\varepsilon} \widehat{\psi}_{m,j} &= \frac{1}{2} \left(\frac{\sigma_{t,j}}{\varepsilon} - \varepsilon \sigma_{a,j} \right) \sum_{k=1}^M \widehat{\psi}_k \omega_k \\ &\quad + \frac{\varepsilon \widehat{Q}_j}{2}, \end{aligned} \tag{2.20}$$

where we ignore the “ \pm ” sign in the numerical fluxes for simplicity, and $\psi_{m,\frac{1}{2}} = f_m$ if $\mu_m > 0$, $\psi_{m,j+\frac{1}{2}} = g_m$ if $\mu_m < 0$. To perform the asymptotic analysis, we start by introducing the following ansatz

$$\psi_m = \sum_{k=0}^{\infty} \varepsilon^k \psi_m^{(k)}$$

for both the cell-edge fluxes $\psi_{m,j+\frac{1}{2}}$ and cell-average fluxes $\psi_{m,j}$ in (2.8). After plugging this ansatz into the HWENO method (2.20), we collect the equations with different orders of ε .

Step 1, $O(\varepsilon^{-1})$ equations: The two $O(\varepsilon^{-1})$ equations are

$$\begin{aligned} \sigma_{t,j} \left(\psi_{m,j}^{(0)} - \frac{1}{2} \sum_{k=1}^M \psi_{k,j}^{(0)} \omega_k \right) &= 0, \\ \sigma_{t,j} \left(\widehat{\psi}_{m,j}^{(0)} - \frac{1}{2} \sum_{k=1}^M \widehat{\psi}_{k,j}^{(0)} \omega_k \right) &= 0. \end{aligned} \tag{2.21}$$

These equations have isotropic solutions

$$\begin{aligned} \psi_{m,j}^{(0)} &= \frac{1}{2} \sum_{k=1}^M \psi_{k,j}^{(0)} \omega_k = \frac{1}{2} \phi_j^{(0)}, \\ \widehat{\psi}_{m,j}^{(0)} &= \frac{1}{2} \sum_{k=1}^M \widehat{\psi}_{k,j}^{(0)} \omega_k = \frac{1}{2} \widehat{\phi}_j^{(0)}, \end{aligned} \tag{2.22}$$

where $\phi_j^{(0)}$ and $\widehat{\phi}_j^{(0)}$ are the average values and first moments of ϕ at cell I_j , respectively.

Step 2, $O(\varepsilon^0)$ equations: The $O(\varepsilon^0)$ equations can be summarized as

$$\begin{aligned} \sigma_{t,j} \left(\psi_{m,j}^{(1)} - \frac{1}{2} \sum_{k=1}^M \psi_{k,j}^{(1)} \omega_k \right) &= -\frac{\mu_m}{\Delta x} \left(\psi_{m,j+\frac{1}{2}}^{(0)} - \psi_{m,j-\frac{1}{2}}^{(0)} \right), \\ \sigma_{t,j} \left(\widehat{\psi}_{m,j}^{(1)} - \frac{1}{2} \sum_{k=1}^M \widehat{\psi}_{k,j}^{(1)} \omega_k \right) &= -\frac{\mu_m}{2\Delta x} \left(\psi_{m,j+\frac{1}{2}}^{(0)} + \psi_{m,j-\frac{1}{2}}^{(0)} - \phi_j^{(0)} \right), \end{aligned} \tag{2.23}$$

where $\psi_{m,\frac{1}{2}}^{(0)} = f_m$ if $\mu_m > 0$, $\psi_{m,J+\frac{1}{2}}^{(0)} = g_m$ if $\mu_m < 0$. Following the linear HWENO reconstruction (2.17a), (2.17b) and (2.22), we have

$$\psi_{m,j+\frac{1}{2}}^{(0)} = \frac{1}{2} \left(\frac{13}{108} \phi_{j-1}^{(0)} + \frac{7}{12} \phi_j^{(0)} + \frac{8}{27} \phi_{j+1}^{(0)} + \frac{25}{54} \widehat{\phi}_{j-1}^{(0)} + \frac{241}{54} \widehat{\phi}_j^{(0)} - \frac{28}{27} \widehat{\phi}_{j+1}^{(0)} \right), \tag{2.24}$$

for $1 \leq j \leq J$ if $\mu_m > 0$, or

$$\psi_{m,j+\frac{1}{2}}^{(0)} = \frac{1}{2} \left(\frac{8}{27} \phi_j^{(0)} + \frac{7}{12} \phi_{j+1}^{(0)} + \frac{13}{108} \phi_{j+2}^{(0)} + \frac{28}{27} \widehat{\phi}_j^{(0)} - \frac{241}{54} \widehat{\phi}_{j+1}^{(0)} - \frac{25}{54} \widehat{\phi}_{j+2}^{(0)} \right), \tag{2.25}$$

for $0 \leq j \leq J - 1$ if $\mu_m < 0$. Multiplying (2.23) by Gauss quadrature weights ω_m , and summing over m , we find that the left sides vanish, and the right sides yield the solvability conditions (after using (2.2), more specifically, $\sum_m \mu_m \omega_m = 0$)

$$for\ 0 = \sum_{m=1}^M \mu_m \psi_{m,j+\frac{1}{2}}^{(0)} \omega_m, \quad 0 \leq j \leq J, \tag{2.26}$$

which must be satisfied for a solution of (2.23) to exist.

We start by considering the case of $j = 0$. The combination of (2.25) and (2.26) leads to

$$0 = \frac{1}{2} \left(\frac{8}{27}\phi_0^{(0)} + \frac{7}{12}\phi_1^{(0)} + \frac{13}{108}\phi_2^{(0)} + \frac{28}{27}\widehat{\phi}_0^{(0)} - \frac{241}{54}\widehat{\phi}_1^{(0)} - \frac{25}{54}\widehat{\phi}_2^{(0)} \right) \sum_{\mu_m < 0} \mu_m \omega_m + \sum_{\mu_m > 0} \mu_m f_m \omega_m. \tag{2.27}$$

Let us define γ as in [24]

$$\gamma = 2 \sum_{\mu_m > 0} \mu_m \omega_m \approx 1.$$

Combined with (2.2), we obtain

$$\sum_{\mu_m > 0} \mu_m \omega_m = \frac{\gamma}{2} \text{ and } \sum_{\mu_m < 0} \mu_m \omega_m = -\frac{\gamma}{2}, \tag{2.28}$$

therefore the Eq. (2.27) yields

$$\frac{8}{27}\phi_0^{(0)} + \frac{7}{12}\phi_1^{(0)} + \frac{13}{108}\phi_2^{(0)} + \frac{28}{27}\widehat{\phi}_0^{(0)} - \frac{241}{54}\widehat{\phi}_1^{(0)} - \frac{25}{54}\widehat{\phi}_2^{(0)} = \frac{4}{\gamma} \sum_{\mu_m > 0} \mu_m f_m \omega_m. \tag{2.29}$$

Next, for any j satisfying $1 \leq j \leq J - 1$ or $j = J$, we follow the similar approach to combine (2.26), (2.24), (2.25) and (2.28) and derive

$$\begin{aligned} & \frac{13}{108}\phi_{j-1}^{(0)} + \frac{7}{12}\phi_j^{(0)} + \frac{8}{27}\phi_{j+1}^{(0)} + \frac{25}{54}\widehat{\phi}_{j-1}^{(0)} + \frac{241}{54}\widehat{\phi}_j^{(0)} - \frac{28}{27}\widehat{\phi}_{j+1}^{(0)} \\ &= \frac{8}{27}\phi_j^{(0)} + \frac{7}{12}\phi_{j+1}^{(0)} + \frac{13}{108}\phi_{j+2}^{(0)} + \frac{28}{27}\widehat{\phi}_j^{(0)} - \frac{241}{54}\widehat{\phi}_{j+1}^{(0)} \\ & \quad - \frac{25}{54}\widehat{\phi}_{j+2}^{(0)}, \quad 1 \leq j \leq J - 1; \end{aligned} \tag{2.30}$$

$$\begin{aligned} & \frac{13}{108}\phi_{J-1}^{(0)} + \frac{7}{12}\phi_J^{(0)} + \frac{8}{27}\phi_{J+1}^{(0)} + \frac{25}{54}\widehat{\phi}_{J-1}^{(0)} + \frac{241}{54}\widehat{\phi}_J^{(0)} - \frac{28}{27}\widehat{\phi}_{J+1}^{(0)} \\ &= \frac{4}{\gamma} \sum_{\mu_m < 0} |\mu_m| g_m \omega_m. \end{aligned} \tag{2.31}$$

Let us define the following cell interface notations:

$$\begin{aligned} \phi_{\frac{1}{2}}^{(0)} &= \frac{8}{27}\phi_0^{(0)} + \frac{7}{12}\phi_1^{(0)} + \frac{13}{108}\phi_2^{(0)} + \frac{28}{27}\widehat{\phi}_0^{(0)} - \frac{241}{54}\widehat{\phi}_1^{(0)} - \frac{25}{54}\widehat{\phi}_2^{(0)}; \\ \phi_{j+\frac{1}{2}}^{(0)} &= \frac{13}{108}\phi_{j-1}^{(0)} + \frac{7}{12}\phi_j^{(0)} + \frac{8}{27}\phi_{j+1}^{(0)} + \frac{25}{54}\widehat{\phi}_{j-1}^{(0)} + \frac{241}{54}\widehat{\phi}_j^{(0)} - \frac{28}{27}\widehat{\phi}_{j+1}^{(0)} \\ &= \frac{8}{27}\phi_j^{(0)} + \frac{7}{12}\phi_{j+1}^{(0)} + \frac{13}{108}\phi_{j+2}^{(0)} + \frac{28}{27}\widehat{\phi}_j^{(0)} - \frac{241}{54}\widehat{\phi}_{j+1}^{(0)} - \frac{25}{54}\widehat{\phi}_{j+2}^{(0)}, \quad 1 \leq j \leq J - 1; \\ \phi_{J+\frac{1}{2}}^{(0)} &= \frac{13}{108}\phi_{J-1}^{(0)} + \frac{7}{12}\phi_J^{(0)} + \frac{8}{27}\phi_{J+1}^{(0)} + \frac{25}{54}\widehat{\phi}_{J-1}^{(0)} + \frac{241}{54}\widehat{\phi}_J^{(0)} - \frac{28}{27}\widehat{\phi}_{J+1}^{(0)}, \end{aligned}$$

which can be denoted as

$$\begin{aligned} \phi_{j+\frac{1}{2}}^{(0)} &= L_1 \left(\phi_j^{(0)}, \phi_{j+1}^{(0)}, \phi_{j+2}^{(0)}, \widehat{\phi}_j^{(0)}, \widehat{\phi}_{j+1}^{(0)}, \widehat{\phi}_{j+2}^{(0)} \right); \quad 0 \leq j \leq J - 1; \\ \phi_{j+\frac{1}{2}}^{(0)} &= L_2 \left(\phi_{j-1}^{(0)}, \phi_j^{(0)}, \phi_{j+1}^{(0)}, \widehat{\phi}_{j-1}^{(0)}, \widehat{\phi}_j^{(0)}, \widehat{\phi}_{j+1}^{(0)} \right); \quad 1 \leq j \leq J; \end{aligned} \tag{2.32}$$

with L_1 and L_2 being two linear operators. In the ghost cells I_0 and I_{J+1} , we use the fifth-order extrapolation to evaluate their cell averages and first moments in this paper, and have

$$\begin{aligned} \phi_0^{(0)} &= \sum_{j=1}^5 c_j \phi_j^{(0)}, & \phi_{J+1}^{(0)} &= \sum_{j=J-4}^J c'_j \phi_j^{(0)}, \\ \widehat{\phi}_0 &= \sum_{j=1}^5 \widehat{c}_j \widehat{\phi}_j^{(0)}, & \widehat{\phi}_{J+1} &= \sum_{j=J-4}^J \widehat{c}'_j \phi_j^{(0)}, \end{aligned} \tag{2.33}$$

where c_j, c'_j, \widehat{c}_j and \widehat{c}'_j are constants computed by Lagrange interpolating. Therefore, by combining the linear relations (2.32) and (2.33), and then inverting them, we can obtain two linear operators L and \widehat{L} , such that

$$\phi_j^{(0)} = L \left(\phi_{\frac{1}{2}}^{(0)}, \dots, \phi_{J+\frac{1}{2}}^{(0)} \right), \quad \widehat{\phi}_j^{(0)} = \widehat{L} \left(\phi_{\frac{1}{2}}^{(0)}, \dots, \phi_{J+\frac{1}{2}}^{(0)} \right), \quad 1 \leq j \leq J.$$

At the end of this step, let us summarize the results that are derived from Eqs. (2.29)–(2.31) and will be used later:

$$\phi_{\frac{1}{2}}^{(0)} = \frac{4}{\gamma} \sum_{\mu_m > 0} \mu_m f_m \omega_m; \tag{2.34a}$$

$$\phi_j^{(0)} = L \left(\phi_{\frac{1}{2}}^{(0)}, \dots, \phi_{J+\frac{1}{2}}^{(0)} \right), \quad 1 \leq j \leq J, \tag{2.34b}$$

$$\widehat{\phi}_j^{(0)} = \widehat{L} \left(\phi_{\frac{1}{2}}^{(0)}, \dots, \phi_{J+\frac{1}{2}}^{(0)} \right), \quad 1 \leq j \leq J, \tag{2.34c}$$

$$\phi_{J+\frac{1}{2}}^{(0)} = \frac{4}{\gamma} \sum_{\mu_m < 0} |\mu_m| g_m \omega_m, \tag{2.34d}$$

and

$$\psi_{m,j+\frac{1}{2}}^{(0)} = \begin{cases} f_m, & j = 0, \quad \mu_m > 0; \\ \frac{1}{2} \phi_{j+\frac{1}{2}}^{(0)}, & \begin{cases} 1 \leq j \leq J, & \mu_m > 0; \\ 0 \leq j \leq J-1, & \mu_m < 0; \end{cases} \\ g_m, & j = J, \quad \mu_m < 0. \end{cases} \tag{2.35}$$

Also, note that the general solutions of (2.23) take the form

$$\psi_{m,j}^{(1)} = \frac{1}{2} \phi_j^{(1)} - \frac{\mu_m}{\sigma_{t,j} \Delta x} (\psi_{m,j+\frac{1}{2}}^{(0)} - \psi_{m,j-\frac{1}{2}}^{(0)}), \quad 1 \leq j \leq J. \tag{2.36}$$

Step 3, $O(\varepsilon^1)$ equations: Next, we consider the $O(\varepsilon^1)$ equations, which take the form

$$\begin{aligned} \sigma_{t,j} \left(\psi_{m,j}^{(2)} - \frac{1}{2} \sum_{k=1}^M \psi_{k,j}^{(2)} \omega_k \right) &= -\frac{\mu_m}{\Delta x} \left(\psi_{m,j+\frac{1}{2}}^{(1)} - \psi_{m,j-\frac{1}{2}}^{(1)} \right) + \frac{1}{2} \left(-\sigma_{a,j} \phi_j^{(0)} + Q_j \right), \\ \sigma_{t,j} \left(\widehat{\psi}_{m,j}^{(2)} - \frac{1}{2} \sum_{k=1}^M \widehat{\psi}_{k,j}^{(2)} \omega_k \right) &= -\frac{\mu_m}{2\Delta x} \left(\psi_{m,j+\frac{1}{2}}^{(1)} + \psi_{m,j-\frac{1}{2}}^{(1)} - 2\psi_{m,j}^{(1)} \right) \\ &\quad + \frac{1}{2} \left(-\sigma_{a,j} \widehat{\phi}_j^{(0)} + \widehat{Q}_j \right). \end{aligned} \tag{2.37}$$

The solvability conditions of these equations are

$$\sum_{m=1}^M \mu_m \psi_{m,j+\frac{1}{2}}^{(1)} \omega_m - \sum_{m=1}^M \mu_m \psi_{m,j-\frac{1}{2}}^{(1)} \omega_m = \Delta x \left(-\sigma_{a,j} \phi_j^{(0)} + Q_j \right), \tag{2.38}$$

$$\sum_{m=1}^M \mu_m \psi_{m,j+\frac{1}{2}}^{(1)} \omega_m + \sum_{m=1}^M \mu_m \psi_{m,j-\frac{1}{2}}^{(1)} \omega_m = 2 \sum_{m=1}^M \mu_m \psi_{m,j}^{(1)} \omega_m + 2\Delta x \left(-\sigma_{a,j} \widehat{\phi}_j^{(0)} + \widehat{Q}_j \right). \tag{2.39}$$

Adding Eq. (2.38) over the j th and $(j + 1)$ th cells, and taking the difference of Eq. (2.39) at cells j and $j + 1$, yield two equalities with the same left side, which leads to the equivalence of their right sides. Therefore, we have

$$\begin{aligned} & \sum_{m=1}^M \mu_m \left(\psi_{m,j+1}^{(1)} - \psi_{m,j}^{(1)} \right) \omega_m + \frac{\Delta x}{2} \left[\sigma_{a,j+1} \left(\phi_{j+1}^{(0)} - 2\widehat{\phi}_{j+1}^{(0)} \right) + \sigma_{a,j} \left(\phi_j^{(0)} + 2\widehat{\phi}_j^{(0)} \right) \right] \\ & = \frac{\Delta x}{2} \left[(Q_{j+1} - 2\widehat{Q}_{j+1}) + (Q_j + 2\widehat{Q}_j) \right], \quad 1 \leq j \leq J - 1. \end{aligned} \tag{2.40}$$

Step 4, diffusion equation: In this last step, we combine the results in the previous steps, and show that the solution $\phi_j^{(0)}$ satisfies an equation which is a consistent numerical discretization of the diffusion equation (2.19).

We first plug in Eqs. (2.34)–(2.36) into Eq. (2.40) and obtain

$$\begin{aligned} & -\frac{1}{3\sigma_{t,j+1}\Delta x} \left(\phi_{j+\frac{3}{2}}^{(0)} - \phi_{j+\frac{1}{2}}^{(0)} \right) + \frac{1}{3\sigma_{t,j}\Delta x} \left(\phi_{j+\frac{1}{2}}^{(0)} - \phi_{j-\frac{1}{2}}^{(0)} \right) \\ & + \frac{\Delta x}{2} \left[\sigma_{a,j+1} \left(\phi_{j+1}^{(0)} - 2\widehat{\phi}_{j+1}^{(0)} \right) + \sigma_{a,j} \left(\phi_j^{(0)} + 2\widehat{\phi}_j^{(0)} \right) \right] \\ & = \frac{\Delta x}{2} \left[(Q_{j+1} - 2\widehat{Q}_{j+1}) + (Q_j + 2\widehat{Q}_j) \right], \quad 1 \leq j \leq J - 1. \end{aligned} \tag{2.41}$$

We consider the Taylor expansion of $\phi(x)$ and $\phi(x) \frac{x-x_j}{\Delta x}$ at any point $x_* \in [x_{j-\frac{1}{2}}, x_{j+\frac{1}{2}}]$, which leads to

$$\begin{aligned} \phi(x) & = \phi_* + \phi'_*(x - x_*) + \frac{\phi''_*}{2}(x - x_*)^2 + O(\Delta x^3), \\ \phi(x) \frac{x - x_j}{\Delta x} & = \phi_* \frac{x_* - x_j}{\Delta x} + \left(\phi'_* \frac{x_* - x_j}{\Delta x} + \frac{\phi_*}{\Delta x} \right) (x - x_*) \\ & + \left(\phi''_* \frac{x_* - x_j}{2\Delta x} + \frac{\phi'_*}{\Delta x} \right) (x - x_*)^2 + O(\Delta x^3). \end{aligned} \tag{2.42}$$

Taking $x_* = x_{j-\frac{1}{2}}$, multiplying (2.42) with $\frac{1}{\Delta x}$, and integrating on the cell I_j yield

$$\begin{aligned} \phi_j & = \phi_{j-\frac{1}{2}} + \frac{\Delta x}{2} \phi'_{j-\frac{1}{2}} + \frac{\Delta x^2}{6} \phi''_{j-\frac{1}{2}} + O(\Delta x^3), \\ \widehat{\phi}_j & = \frac{\Delta x}{12} \phi'_{j-\frac{1}{2}} - \frac{\Delta x^2}{12} \phi''_{j-\frac{1}{2}} + O(\Delta x^3), \end{aligned}$$

following (2.4) and (2.5), hence

$$\phi_j - 2\widehat{\phi}_j = \phi_{j-\frac{1}{2}} + \frac{\Delta x}{3} \phi'_{j-\frac{1}{2}} + \frac{\Delta x^2}{3} \phi''_{j-\frac{1}{2}} + O(\Delta x^3). \tag{2.43}$$

Similarly, we can take $x_* = x_{j+\frac{1}{2}}$ and obtain

$$\phi_j + 2\widehat{\phi}_j = \phi_{j+\frac{1}{2}} - \frac{\Delta x}{3}\phi'_{j+\frac{1}{2}} + \frac{\Delta x^2}{3}\phi''_{j+\frac{1}{2}} + O(\Delta x^3).$$

Hence, the Eq. (2.41) becomes

$$\begin{aligned} & -\frac{1}{3\sigma_{t,j+\frac{1}{2}}\Delta x}(\phi_{j+\frac{3}{2}}^{(0)} - \phi_{j+\frac{1}{2}}^{(0)}) + \frac{1}{3\sigma_{t,j}\Delta x}(\phi_{j+\frac{1}{2}}^{(0)} - \phi_{j-\frac{1}{2}}^{(0)}) \\ & + \frac{\Delta x}{2}(\sigma_{a,j+1}\phi_{j+\frac{1}{2}}^{(0)} + \sigma_{a,j}\phi_{j+\frac{1}{2}}^{(0)}) + O(\Delta x^2) \\ & = \Delta x Q_{j+\frac{1}{2}} + O(\Delta x^3), \quad 1 \leq j \leq J-1, \end{aligned} \tag{2.44}$$

where the right side of equation utilized the equality

$$(Q_{j+1} - 2\widehat{Q}_{j+1}) + (Q_j + 2\widehat{Q}_j) = 2Q_{j+\frac{1}{2}} + O(\Delta x^2),$$

derived in the similar way. Equation (2.44), combined with the boundary conditions

$$\phi_{\frac{1}{2}}^{(0)} = \frac{4}{\gamma} \sum_{\mu_m > 0} \mu_m f_m \omega_m, \quad \text{and} \quad \phi_{J+\frac{1}{2}}^{(0)} = \frac{4}{\gamma} \sum_{\mu_m < 0} |\mu_m| g_m \omega_m, \tag{2.45}$$

provides a consistent numerical discretization of the diffusion equation (2.19).

In summary, we obtain the following expression for the cell-edge angular fluxes

$$\psi_{m,j+\frac{1}{2}} = \begin{cases} f_m, & j = 0, \mu_m > 0 \\ \frac{2}{\gamma} \sum_{\mu_m > 0} \mu_m f_m \omega_m, & j = 0, \mu_m < 0 \\ \frac{1}{2}\phi_{j+\frac{1}{2}}^{(0)}, & 1 \leq j \leq J-1 \\ \frac{2}{\gamma} \sum_{\mu_m < 0} |\mu_m| g_m \omega_m, & j = J, \mu_m > 0 \\ g_m, & j = J, \mu_m < 0 \end{cases} + O(\varepsilon), \tag{2.46}$$

with $\phi_{\frac{1}{2}}^{(0)}$ and $\phi_{J+\frac{1}{2}}^{(0)}$ defined in (2.45), and $\phi_{j+\frac{1}{2}}^{(0)}$ being the solution of (2.44). For the cell-average angular fluxes, we have

$$\psi_{m,j} = \frac{1}{2}L \left(\phi_{\frac{1}{2}}^{(0)}, \dots, \phi_{J+\frac{1}{2}}^{(0)} \right) + O(\varepsilon),$$

with L being the inverse operator to convert the cell interface values into the cell average values. Therefore, when taking the limit as ε approaches zero, the numerical solution $\psi_{m,j+\frac{1}{2}}$ reduces to the solution of the diffusion equation (2.19), which satisfies the stable and consistent method (2.44). In addition, Eq. (2.18) is also achieved. This is the AP property that is desired for the finite volume HWENO method.

3 Multidimensional S_N Transport Equation

In this section, we will discuss the finite volume HWENO FSM for multi-dimensional S_N transport equation (1.1) with isotropic scattering neutron source. Two dimensions will be

used as an example to describe the HWENO FSM method, and the proposed method can be directly extended to any dimension. We consider the following two-dimensional equation

$$\begin{aligned} &\mu_m \frac{\partial}{\partial x} \psi(x, y, \mu_m, \eta_n) + \eta_n \frac{\partial}{\partial y} \psi(x, y, \mu_m, \eta_n) + \frac{\sigma_t}{\varepsilon} \psi(x, y, \mu_m, \eta_n) \\ &= \frac{1}{4} \left(\frac{\sigma_t}{\varepsilon} - \varepsilon \sigma_a \right) \phi(x, y) + \frac{\varepsilon}{4} Q(x, y), \quad (x, y) \in \Omega, \quad (\mu_m, \eta_n) \in [-1, 1] \times [-1, 1], \end{aligned} \tag{3.1}$$

$$\psi(x, y, \mu_m, \eta_n) = f(x, y, \mu_m, \eta_n), \quad (x, y) \in \Gamma^-, \quad (\mu_m, \eta_n) \in [-1, 1] \times [-1, 1], \tag{3.2}$$

where μ_m and η_n represent cosine values of the angles between the neutron direction and x -axis and y -axis, respectively. Here ϕ and ψ are the scalar flux and angular flux with

$$\phi(x, y) = \iint_{[-1,1] \times [-1,1]} \psi(x, y, \mu, \eta) d\mu d\eta = \sum_{m,n=1}^M \omega_m \omega_n \psi(x, y, \mu_m, \eta_n),$$

where ω_m and ω_n are the level symmetric quadrature weights.

Assume the computational domain has been divided into cells $I_{i,j} = J_i \times K_j = [x_{i-\frac{1}{2}}, x_{i+\frac{1}{2}}] \times [y_{j-\frac{1}{2}}, y_{j+\frac{1}{2}}]$, with $i = 1, \dots, N_x, j = 1, \dots, N_y$. We denote the cell center as $(x_i, y_j) = ((x_{i-\frac{1}{2}} + x_{i+\frac{1}{2}})/2, (y_{j-\frac{1}{2}} + y_{j+\frac{1}{2}})/2)$ and the mesh size as $\Delta x_i = x_{i+\frac{1}{2}} - x_{i-\frac{1}{2}}, \Delta y_j = y_{j+\frac{1}{2}} - y_{j-\frac{1}{2}}$. The cell average and first moments of the unknown are denoted as

$$\begin{aligned} \psi_{i,j}^{m,n} &= \frac{1}{\Delta x_i \Delta y_j} \iint_{I_{i,j}} \psi(x, y, \mu_m, \eta_n) dx dy, \\ \widehat{\psi}_{i,j}^{m,n} &= \frac{1}{\Delta x_i \Delta y_j} \iint_{I_{i,j}} \psi(x, y, \mu_m, \eta_n) \frac{x - x_i}{\Delta x_i} dx dy, \\ \widetilde{\psi}_{i,j}^{m,n} &= \frac{1}{\Delta x_i \Delta y_j} \iint_{I_{i,j}} \psi(x, y, \mu_m, \eta_n) \frac{y - y_j}{\Delta y_j} dx dy, \\ \widehat{\widetilde{\psi}}_{i,j}^{m,n} &= \frac{1}{\Delta x_i \Delta y_j} \iint_{I_{i,j}} \psi(x, y, \mu_m, \eta_n) \frac{x - x_i}{\Delta x_i} \frac{y - y_j}{\Delta y_j} dx dy. \end{aligned} \tag{3.3}$$

For simplicity, we ignore the superscript m, n without causing any confusion. Similarly, we can define the cell average and moments of ϕ as $\phi_{i,j}, \widehat{\phi}_{i,j}, \widetilde{\phi}_{i,j}, \widehat{\widetilde{\phi}}_{i,j}$, and those of Q as $Q_{i,j}, \widehat{Q}_{i,j}, \widetilde{Q}_{i,j}, \widehat{\widetilde{Q}}_{i,j}$. We multiply (3.1) by $\frac{1}{\Delta x_i \Delta y_j}, \frac{x - x_i}{\Delta x_i^2 \Delta y_j}, \frac{y - y_j}{\Delta x_i \Delta y_j^2}$ and $\frac{x - x_i}{\Delta x_i^2} \frac{y - y_j}{\Delta y_j^2}$, respectively, and then integrate them on the cell $I_{i,j}$. Applying integration by parts and replacing the cell interface values by the Godunov numerical flux as discussed in one-dimensional setting in Sect. 2.1, we have the following HWENO discretization

$$\begin{aligned} &\frac{\mu_m}{\Delta x_i \Delta y_j} \int_{K_j} [\psi^\pm(x_{i+\frac{1}{2}}, y, \mu_m, \eta_n) - \psi^\pm(x_{i-\frac{1}{2}}, y, \mu_m, \eta_n)] dy \\ &+ \frac{\eta_n}{\Delta x_i \Delta y_j} \int_{J_i} [\psi^\pm(x, y_{j+\frac{1}{2}}, \mu_m, \eta_n) - \psi^\pm(x, y_{j-\frac{1}{2}}, \mu_m, \eta_n)] dx \\ &+ \frac{\sigma_{t,ij}}{\varepsilon} \psi_{i,j}^{m,n} = \frac{1}{4} \left(\frac{\sigma_{t,ij}}{\varepsilon} - \varepsilon \sigma_{a,ij} \right) \sum_{k,l=1}^M \psi_{i,j}^{k,l} \omega_k \omega_l + \frac{\varepsilon}{4} Q_{i,j}, \end{aligned} \tag{3.4}$$

$$\frac{\mu_m}{2\Delta x_i \Delta y_j} \int_{K_j} [\psi^\pm(x_{i+\frac{1}{2}}, y, \mu_m, \eta_n) + \psi^\pm(x_{i-\frac{1}{2}}, y, \mu_m, \eta_n)] dy - \frac{\mu_m}{\Delta x_i} \psi_{i,j}^{m,n}$$

$$\begin{aligned}
 &+ \frac{\eta_n}{\Delta x_i \Delta y_j} \int_{J_i} \frac{x - x_i}{\Delta x_i} [\psi^\pm(x, y_{j+\frac{1}{2}}, \mu_m, \eta_n) - \psi^\pm(x, y_{j-\frac{1}{2}}, \mu_m, \eta_n)] dx \\
 &+ \frac{\sigma_{t,ij}}{\varepsilon} \widehat{\psi}_{i,j}^{m,n} = \frac{1}{4} \left(\frac{\sigma_{t,ij}}{\varepsilon} - \varepsilon \sigma_{a,ij} \right) \sum_{k,l=1}^M \widehat{\psi}_{i,j}^{k,l} \omega_k \omega_l + \frac{\varepsilon}{4} \widehat{Q}_{i,j}, \tag{3.5}
 \end{aligned}$$

$$\begin{aligned}
 &\frac{\mu_m}{\Delta x_i \Delta y_j} \int_{K_j} \frac{y - y_j}{\Delta y_j} [\psi^\pm(x_{i+\frac{1}{2}}, y, \mu_m, \eta_n) - \psi^\pm(x_{i-\frac{1}{2}}, y, \mu_m, \eta_n)] dy \\
 &+ \frac{\eta_n}{2\Delta x_i \Delta y_j} \int_{J_i} [\psi^\pm(x, y_{j+\frac{1}{2}}, \mu_m, \eta_n) + \psi^\pm(x, y_{j-\frac{1}{2}}, \mu_m, \eta_n)] dx - \frac{\eta_n}{\Delta y_j} \psi_{i,j}^{m,n} \\
 &+ \frac{\sigma_{t,ij}}{\varepsilon} \widetilde{\psi}_{i,j}^{m,n} = \frac{1}{4} \left(\frac{\sigma_{t,ij}}{\varepsilon} - \varepsilon \sigma_{a,ij} \right) \sum_{k,l=1}^M \widetilde{\psi}_{i,j}^{k,l} \omega_k \omega_l + \frac{\varepsilon}{4} \widetilde{Q}_{i,j}, \tag{3.6}
 \end{aligned}$$

$$\begin{aligned}
 &\frac{\mu_m}{2\Delta x_i \Delta y_j} \int_{K_j} \frac{y - y_j}{\Delta y_j} [\psi^\pm(x_{i+\frac{1}{2}}, y, \mu_m, \eta_n) + \psi^\pm(x_{i-\frac{1}{2}}, y, \mu_m, \eta_n)] dy - \frac{\mu_m}{\Delta x_i} \widetilde{\psi}_{i,j}^{m,n} \\
 &+ \frac{\eta_n}{2\Delta x_i \Delta y_j} \int_{J_i} \frac{x - x_i}{\Delta x_i} [\psi^\pm(x, y_{j+\frac{1}{2}}, \mu_m, \eta_n) + \psi^\pm(x, y_{j-\frac{1}{2}}, \mu_m, \eta_n)] dx - \frac{\eta_n}{\Delta y_j} \widehat{\psi}_{i,j}^{m,n} \\
 &+ \frac{\sigma_{t,ij}}{\varepsilon} \widehat{\psi}_{i,j}^{m,n} = \frac{1}{4} \left(\frac{\sigma_{t,ij}}{\varepsilon} - \varepsilon \sigma_{a,ij} \right) \sum_{k,l=1}^M \widehat{\psi}_{i,j}^{k,l} \omega_k \omega_l + \frac{\varepsilon}{4} \widehat{Q}_{i,j}, \tag{3.7}
 \end{aligned}$$

where the numerical flux $\psi^\pm(x_{i\pm\frac{1}{2}}, y, \mu_m, \eta_n)$ is chosen to ψ^+ when $\mu_m > 0$ and ψ^- otherwise. Similarly, the numerical flux $\psi^\pm(x, y_{j\pm\frac{1}{2}}, \mu_m, \eta_n)$ is chosen to ψ^+ when $\eta_n > 0$ and ψ^- otherwise. The integrals of the flux over K_j or J_i are evaluated via the HWENO reconstruction to be discussed in the following subsection.

3.1 HWENO Reconstruction in 2D

We can use the dimension-by-dimension strategy to reconstruct these integrals in the HWENO method (3.4)–(3.7), and refer the detailed discussion to [54]. The procedure of these reconstructions is sketched as follows. Again, for ease of presentation, we assume the uniform mesh with $\Delta x_i = \Delta x$, $\Delta y_j = \Delta y$ in the description. We denote $\psi^{m,n}(x, y) = \psi(x, y, \mu_m, \eta_n)$ and ignore the superscript (m, n) below without causing any confusion.

- In the x -direction, we perform the one-dimensional HWENO reconstruction which was described in Sect. 2.1. Therefore, from $\{\psi_{l,j}, \widehat{\psi}_{l,j}\}_{l=i-1}^{i+1}$, we can obtain $\frac{1}{\Delta y} \int_{K_j} \psi^\pm(x_{i\pm\frac{1}{2}}, y) dy$, which is the point value in the x -direction and the cell-average in the y -direction. Similarly, we can use the values $\{\widetilde{\psi}_{l,j}, \widehat{\widetilde{\psi}}_{l,j}\}_{l=i-1}^{i+1}$ to reconstruct $\frac{1}{\Delta y} \int_{K_j} \psi^\pm(x_{i\pm\frac{1}{2}}, y) \frac{y-y_j}{\Delta y} dy$. Note that either “+” or “-” sign is taken, depending on whether μ_m is negative or positive.
- In the y -direction, we perform the one-dimensional HWENO reconstruction which was described in Sect. 2.1. Therefore, from $\{\psi_{i,l}, \widetilde{\psi}_{i,l}\}_{l=j-1}^{j+1}$, we can obtain $\frac{1}{\Delta x} \int_{J_i} \psi(x, y_{j\pm\frac{1}{2}}) dx$, which is the point value in the y -direction and the cell-average in the x -direction. Similarly, we can use the values $\{\widehat{\psi}_{i,l}, \widehat{\widetilde{\psi}}_{i,l}\}_{l=j-1}^{j+1}$ to reconstruct $\frac{1}{\Delta x} \int_{J_i} \psi(x, y_{j\pm\frac{1}{2}}) \frac{x-x_i}{\Delta x} dx$. Note that either “+” or “-” sign is taken, depending on whether η_n is negative or positive.

3.2 Fast Sweeping Idea to Solve a Global Linear System in 2D

The proposed two-dimensional HWENO scheme for the linear transport equation (3.1), takes the form of (3.4)–(3.7), combined with the HWENO reconstruction to evaluate the fluxes. This is a large system involving the flux term (coupling in x and y directions) on the left side and the summation term (coupling in μ and η directions) on the right side. As in one-dimensional case, the fast sweeping idea is adopted to solve this system efficiently. Let us first denote the right-hand side term of the four equations in (3.4)–(3.7) as $S_{i,j}$, $\widehat{S}_{i,j}$, $\widetilde{S}_{i,j}$ and $\widehat{\widehat{S}}_{i,j}$, respectively. We summarize the flowchart of HWENO FSM for the S_N equation in 2D as follows.

Step 1. Initialization: We take 0 as the initial values of the unknowns: $\psi_{i,j}^{m,n}$, $\widehat{\psi}_{i,j}^{m,n}$, $\widetilde{\psi}_{i,j}^{m,n}$ and $\widehat{\widehat{\psi}}_{i,j}^{m,n}$ for all m, n, i and j . Then we can evaluate $S_{i,j}$, $\widehat{S}_{i,j}$, $\widetilde{S}_{i,j}$ and $\widehat{\widehat{S}}_{i,j}$.

Step 2. Gauss-Seidel iteration with alternating sweeps. We sweep the whole domain with the following four alternating orderings repeatedly for all m and n :

- (I) $i = 1 \rightarrow N_x, j = 1 \rightarrow N_y$: if $\mu_m > 0$ and $\eta_n > 0$, solve the system (3.4)–(3.7) with the appropriate boundary conditions with this order of i, j . After updating the approximations $\psi_{i,j}^{m,n}$, $\widehat{\psi}_{i,j}^{m,n}$, $\widetilde{\psi}_{i,j}^{m,n}$ and $\widehat{\widehat{\psi}}_{i,j}^{m,n}$ in the cell $I_{i,j}$, we can apply HWENO reconstruction to obtain the cell-edge flux fluxes $\frac{1}{\Delta y} \int_{K_j} \psi^-(x_{i+\frac{1}{2}}, y) dy$ and $\frac{1}{\Delta x} \int_{J_i} \psi^-(x, y_{j+\frac{1}{2}}) dx$ based on the most updated values of the unknowns.
- (II) $i = N_x \rightarrow 1, j = 1 \rightarrow N_y$: if $\mu_m < 0$ and $\eta_n > 0$, solve the system (3.4)–(3.7) with the appropriate boundary conditions with this order of i, j . After updating the approximations $\psi_{i,j}^{m,n}$, $\widehat{\psi}_{i,j}^{m,n}$, $\widetilde{\psi}_{i,j}^{m,n}$ and $\widehat{\widehat{\psi}}_{i,j}^{m,n}$ in the cell $I_{i,j}$, we can apply HWENO reconstruction to obtain the cell-edge flux fluxes $\frac{1}{\Delta y} \int_{K_j} \psi^+(x_{i-\frac{1}{2}}, y) dy$ and $\frac{1}{\Delta x} \int_{J_i} \psi^-(x, y_{j+\frac{1}{2}}) dx$ based on the most updated values of the unknowns.
- (III) $i = 1 \rightarrow N_x, j = N_y \rightarrow 1$: if $\mu_m > 0$ and $\eta_n < 0$, solve the system (3.4)–(3.7) with the appropriate boundary conditions with this order of i, j . After updating the approximations $\psi_{i,j}^{m,n}$, $\widehat{\psi}_{i,j}^{m,n}$, $\widetilde{\psi}_{i,j}^{m,n}$ and $\widehat{\widehat{\psi}}_{i,j}^{m,n}$ in the cell $I_{i,j}$, we can apply HWENO reconstruction to obtain the cell-edge flux fluxes $\frac{1}{\Delta y} \int_{K_j} \psi^-(x_{i+\frac{1}{2}}, y) dy$ and $\frac{1}{\Delta x} \int_{J_i} \psi^+(x, y_{j-\frac{1}{2}}) dx$ based on the most updated values of the unknowns.
- (IV) $i = N_x \rightarrow 1, j = N_y \rightarrow 1$: if $\mu_m < 0$ and $\eta_n < 0$, solve the system (3.4)–(3.7) with the appropriate boundary conditions with this order of i, j . After updating the approximations $\psi_{i,j}^{m,n}$, $\widehat{\psi}_{i,j}^{m,n}$, $\widetilde{\psi}_{i,j}^{m,n}$ and $\widehat{\widehat{\psi}}_{i,j}^{m,n}$ in the cell $I_{i,j}$, we can apply HWENO reconstruction to obtain the cell-edge flux fluxes $\frac{1}{\Delta y} \int_{K_j} \psi^+(x_{i-\frac{1}{2}}, y) dy$ and $\frac{1}{\Delta x} \int_{J_i} \psi^+(x, y_{j-\frac{1}{2}}) dx$ based on the most updated values of the unknowns.

At the boundary of the computational domain, high-order extrapolations are used to compute the values at the ghost cells, which are needed for the HWENO reconstruction near the boundary. After repeating this process for all m, n directions, we can compute scalar flux ϕ from $\psi^{m,n}$ via Gauss quadrature, and update $S_{i,j}$ etc. This completes one Gauss-Seidel iteration.

Step 3. Convergence: Repeat the Gauss-Seidel iteration until the convergence criteria is satisfied. In this paper, if the scalar flux satisfies

$$\delta = \|\phi^{new} - \phi^{old}\|_{L_1} < 10^{-14},$$

for two consecutive iteration steps, we stop the iteration.

Remark 3.1 In some two-dimensional numerical experiments, we observed that the proposed HWENO FSM may not converge to machine epsilon, i.e., $\delta = \|\phi^{new} - \phi^{old}\|_{L_1}$ will not decrease to 10^{-14} . The same phenomenon has also been observed in the application of HWENO FSM method to other systems as reported in [39, 40]. This may be related to high-order extrapolation for the ghost cells near the boundary. For example, if the low order extrapolation is used for ghost cells only, the proposed method works well in these numerical examples. However, this will degenerate the high-order accuracy of the proposed method. To fix this, we propose to keep the high-order extrapolation while update the solution by

$$\psi_{i,j}^{new} = \omega \psi_{i,j}^{new} + (1 - \omega) \psi_{i,j}^{old}, \quad 0 < \omega \leq 1,$$

which is shown numerically to yield good convergence, although it may slightly increase the iteration numbers. Numerically, one observes that $\omega = 0.85$ is the optimal choice and will be used in our 2D numerical examples.

If the standard Gauss-Seidel iteration method (without alternative sweeping) is used instead, we observe numerically that the parameter $\omega = 0.5$ is required for convergence, even for 1D problems. On the other hand, the FSM does not need the parameter ω for 1D problems. See Sect. 4 for the numerical results.

4 Numerical Results

We present extensive one-dimensional and two-dimensional numerical results on different model problems, to demonstrate the diffusion limit and order of accuracy of the proposed HWENO fast sweeping method in the finite volume framework. In all the numerical examples, $\tilde{\varepsilon}$ in (2.15) is taken as 10^{-6} unless otherwise specified. The number of grid points is assumed to be $N_x = N_y = N$ for 2D examples. We use “iter” to denote the iteration numbers in the tables.

4.1 One-Dimensional Problem with Vacuum Boundary

Example 1 (*Accuracy test with manufactured solution*). In the first example, we consider a slab with the vacuum boundary on both sides to test the accuracy of the proposed HWENO method. The specifications of the problem are given as

$$L = 1, \quad \sigma_t = 1, \quad \sigma_a = 0.8, \quad Q = \frac{2}{\varepsilon} [(3x^2 - 12x^3 + 15x^4 - 6x^5)\mu_m] + 2\sigma_a x^3 (1 - x)^3,$$

where L is the slab thickness. The manufactured exact solution of the linear transport equation is given by [42]

$$\psi(x, \mu_m) = x^3 (1 - x)^3.$$

The Gauss-Legendre S_{12} quadrature set is used in the angular discretization. We have run the simulations for various choices of ε . In Table 1, we show the numerical errors, the corresponding order of accuracy and CPU times of the HWENO method with the hybrid strategy discussed in Remark 2.2. Here we only report the cell-average errors to save space, and similar behavior has been observed for the first order moment. Note that the expected high-order accuracy has been observed for all choices of ε . The numerical solutions and iteration history ($\|\phi^n - \phi^{n-1}\|_{L_1}$) with spatial size $\Delta x = 0.1$, $\varepsilon = 0.01, 0.001$ and 0.0001 , compared with the corresponding reference solutions, are plotted in Fig. 2, from which we can observe a good match of the numerical solution even for small ε .

Table 1 Example 1.

N	L_1 error	order	L_∞ error	order	iter	time
$\varepsilon = 1$						
10	1.26e-05	-	5.53e-05	-	60	0.006
20	1.84e-07	6.09	1.52e-06	5.18	56	0.002
40	1.96e-09	6.55	3.13e-08	5.60	52	0.003
80	1.80e-11	6.76	5.61e-10	5.800	49	0.009
160	1.69e-13	6.73	9.41e-12	5.89	47	0.013
$\varepsilon = 0.1$						
10	5.59e-05	-	2.59e-04	-	886	0.02
20	9.91e-07	5.81	8.23e-06	4.97	884	0.04
40	1.40e-08	6.14	1.98e-07	5.37	883	0.04
80	1.80e-10	6.28	4.17e-09	5.57	882	0.05
160	2.06e-12	6.44	7.91e-11	5.72	882	0.13
$\varepsilon = 0.01$						
10	7.94e-05	-	3.40e-04	-	60976	1.41
20	1.68e-06	5.55	1.57e-05	4.43	60976	1.76
40	2.98e-08	5.82	5.36e-07	4.87	60969	2.81
80	5.88e-10	5.66	1.48e-08	5.17	60973	4.31
160	1.25e-11	5.54	3.55e-10	5.38	60970	7.15

The errors, order of accuracy and CPU time of HWENO method with the hybrid strategy

We have also tested the HWENO method without the hybrid strategy, and summarized the comparison of their CPU times and iteration numbers in Table 2. Note that the recorded time listed in Table 2 is the total CPU times of all the simulations with $N = 10, 20, \dots, 160$ and $\varepsilon = 0.01$. For this example, it can be observed that the hybrid strategy saves 70% of CPU time.

As mentioned in the introduction, we have also tested the fifth-order finite difference HWENO method and did not observe AP property numerically. For comparison, we have plotted the numerical results of finite difference HWENO method for this example in Fig. 3. Obvious numerical errors can be seen on coarse meshes when ε becomes smaller (for example, $\varepsilon = 0.001$ or 0.0001), while the numerical errors of finite volume HWENO method remain small for all ranges of ε .

To compare FSM and the standard Gauss-Seidel (GS) iteration (without alternative sweeping), we compare the performance of two methods, including numerical errors, convergence order, iteration numbers and CPU times, in Table 3. The numerical results for FSM are reported on the left side, and those of GS iteration are reported on the right side. Note that the GS iteration requires a smaller value of $\omega (=0.5)$ for convergence, where ω is the parameter reported in Remark 3.1. For comparison, we also set $\omega = 0.5$ in the simulation of FSM. We can observe the iteration numbers of FSM are smaller than GS iteration on the same meshes, and the FSM costs less CPU time than GS iteration, even with $\omega = 0.5$. Note that the FSM can take a larger $\omega (=1)$ with the numerical results reported in Table 1, which further reduces the computational time.

Example 2 A slab with the vacuum boundary on both sides with

$$L = 1, \quad \sigma_t = 1, \quad \sigma_a = 0.8, \quad Q = 1,$$

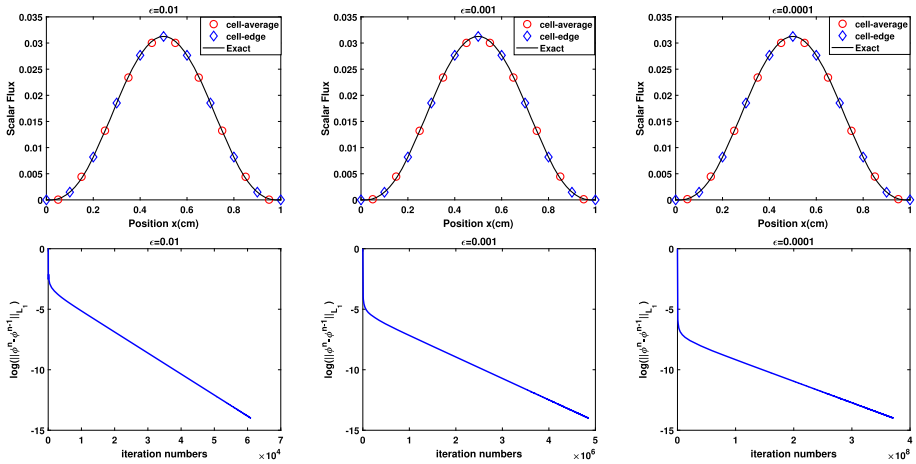


Fig. 2 Example 1 with $\Delta x = 0.1$. Numerical solutions (top); Iteration history (bottom); $\varepsilon = 0.01$ (left); $\varepsilon = 0.001$ (middle); $\varepsilon = 0.0001$ (right)

Table 2 The CPU times of the HWENO method with or without the hybrid strategy for all the Examples.

Test	With hybrid strategy		Without hybrid strategy		Ratio
	iter	time	iter	time	
1	–	17.47	–	62.73	27.85%
2	–	83.95	–	452.35	18.55%
3	4726476	123.74	4727810	246.88	50.12%
4	4456737	153.51	4457270	229.46	66.90%
5	5311441	209.95	5311566	456.40	46.00%
6	5680997	221.31	5681346	480.77	46.03%

“iter” and “time” denote the iteration numbers and CPU time, respectively. The “ratio” represents the ratio of the CPU time of method with hybrid strategy over that without hybrid strategy

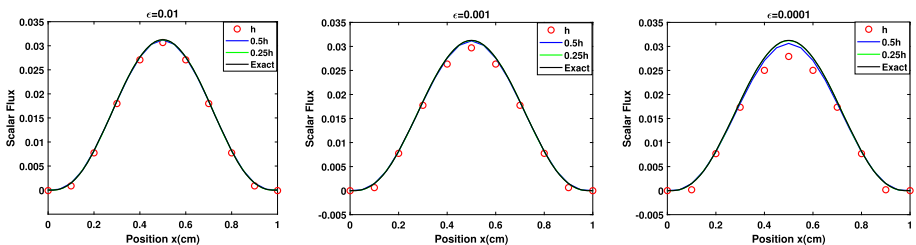


Fig. 3 Numerical solutions of Example 1 with $h = \Delta x = 0.1$ if finite difference HWENO method is used. $\varepsilon = 0.01$ (left), $\varepsilon = 0.001$ (middle), $\varepsilon = 0.0001$ (right)

is considered. Again, the Gauss-Legendre S_{12} quadrature set is used in the angular discretization. The analytical solution can be obtained following the approach discussed in [44]. We have run the simulations for various choices of ε . In Table 4, we show the numerical errors, order of accuracy, and CPU times of the HWENO method with the hybrid strategy. Here we only report the errors of cell-average to save space, and similar behavior has been observed

Table 3 Example 1. Comparison of the two iteration methods with $\omega = 0.5$:

$\varepsilon = 1$, FSM		$\varepsilon = 1$, GS iteration										
N	L_1 error	order	L_∞ error	order	iter	time	L_1 error	order	L_∞ error	order	iter	time
10	1.26e-05	-	5.53e-05	-	122	0.008	1.26e-05	-	5.53e-05	-	187	0.009
20	1.84e-07	6.09	1.52e-06	5.18	184	0.010	1.8e-07	6.09	1.52e-06	5.18	255	0.016
40	1.96e-09	6.55	3.13e-08	5.60	308	0.017	1.96e-09	6.55	3.13e-08	5.60	344	0.020
80	1.80e-11	6.76	5.61e-10	5.80	552	0.040	1.80e-11	6.76	5.61e-10	5.80	647	0.046
160	1.71e-13	6.71	9.40e-12	5.90	1032	0.162	1.72e-13	6.71	9.39e-12	5.90	1241	0.194
$\varepsilon = 0.1$, FSM		$\varepsilon = 0.1$, GS iteration										
N	L_1 error	order	L_∞ error	order	iter	time	L_1 error	order	L_∞ error	order	iter	time
10	5.59e-05	-	2.59e-04	-	2438	0.09	5.59e-05	-	2.59e-04	-	2547	0.10
20	9.91e-07	5.81	8.23e-06	4.97	2900	0.15	9.91e-07	5.81	8.23e-06	4.97	3110	0.15
40	1.40e-08	6.14	1.98e-07	5.37	3816	0.22	1.40e-08	6.14	1.98e-07	5.37	4230	0.31
80	1.80e-10	6.28	4.17e-09	5.57	5624	0.52	1.8e-10	6.28	4.17e-09	5.57	6444	0.6
160	2.00e-12	6.48	7.90e-11	5.72	9191	1.47	1.99e-12	6.49	7.90e-11	5.72	10813	2.02
$\varepsilon = 0.01$, FSM		$\varepsilon = 0.01$, GS iteration										
N	L_1 error	order	L_∞ error	order	iter	time	L_1 error	order	L_∞ error	order	iter	time
10	7.94e-05	-	3.40e-04	-	141590	3.8406	7.94e-05	-	3.40e-04	-	142440	4.21
20	1.68e-06	5.55	1.57e-05	4.43	145030	4.9381	1.68e-06	5.55	1.57e-05	4.43	146650	5.43
40	2.98e-08	5.82	5.36e-07	4.87	151930	7.7876	2.98e-08	5.82	5.36e-07	4.87	155130	8.21
80	5.86e-10	5.66	1.48e-08	5.17	165690	13.544	5.86e-10	5.66	1.48e-08	5.17	172050	14.96
160	1.09e-11	5.73	3.55e-10	5.38	193030	29.538	1.09e-11	5.74	3.55e-10	5.38	205620	31.23

The errors of numerical solution, convergence rate and iteration numbers

Table 4 Example 2.

N	L_1 error	order	L_∞ error	order	iter	time
$\varepsilon = 1$						
10	1.80e-05	–	4.60e-05	–	53	0.0020
20	4.07e-07	5.47	2.19e-06	4.38	50	0.0020
40	5.50e-09	6.20	6.03e-08	5.18	46	0.0022
80	5.69e-11	6.59	1.25e-09	5.58	43	0.0029
160	5.13e-13	6.79	2.27e-11	5.78	41	0.0071
$\varepsilon = 0.1$						
10	2.18e-04	–	8.09e-04	–	882	0.023
20	6.13e-05	1.82	3.46e-04	1.22	882	0.02
40	8.90e-06	2.78	8.64e-05	2.00	883	0.03
80	5.24e-07	4.08	9.11e-06	3.24	883	0.04
160	1.39e-08	5.22	4.41e-07	4.36	883	0.08
320	2.16e-10	6.01	1.27e-08	5.11	883	0.16
$\varepsilon = 0.01$						
10	4.62e-05	–	1.71e-04	–	61034	1.62
20	3.17e-05	0.54	1.78e-04	-0.05	61051	1.58
40	1.89e-05	0.74	1.48e-04	0.26	61057	2.23
80	9.46e-06	1.00	9.08e-05	0.70	61059	4.27
160	3.57e-06	1.40	4.29e-05	1.08	61062	7.01
320	7.85e-07	2.18	1.33e-05	1.68	61063	12.6
640	7.26e-08	3.43	1.87e-06	2.83	61066	22.0
1280	2.76e-09	4.71	1.13e-07	4.04	61068	45.4
2560	6.36e-11	5.43	3.74e-09	4.94	61058	91.5

The errors, order of accuracy and CPU time of HWENO method with the hybrid strategy

for the first order moment. We can observe that the expected high-order accuracy has been observed for all choices of ε . The numerical solutions and iteration history with spatial size $\Delta x = 0.1$, $\varepsilon = 0.01$ and 0.001 , compared with the corresponding reference solutions, are plotted in Fig. 4, from which we can observe a good match of numerical solutions even for small ε . From the total CPU times (combination of $N = 10 \sim 1280$) comparison of HWENO method with/without the hybrid strategy in Table 2, we observe an 80% saving of CPU time when the hybrid strategy is used. In Table 5, we list the numerical results of FSM and the standard GS iteration, including the numerical errors, convergence order, iteration numbers and CPU times. As in Example 1, we can observe that FSM is more efficient than GS iteration.

As ε decreases the problem becomes thick and diffusive, and its asymptotic solution should be the same as the solution of the corresponding diffusion equation. In Table 6, we list the errors between numerical solution of S_N equation with different ε and the exact solution of the diffusion equation, from which we can observe the errors decay at the expected rate of $O(\varepsilon)$.

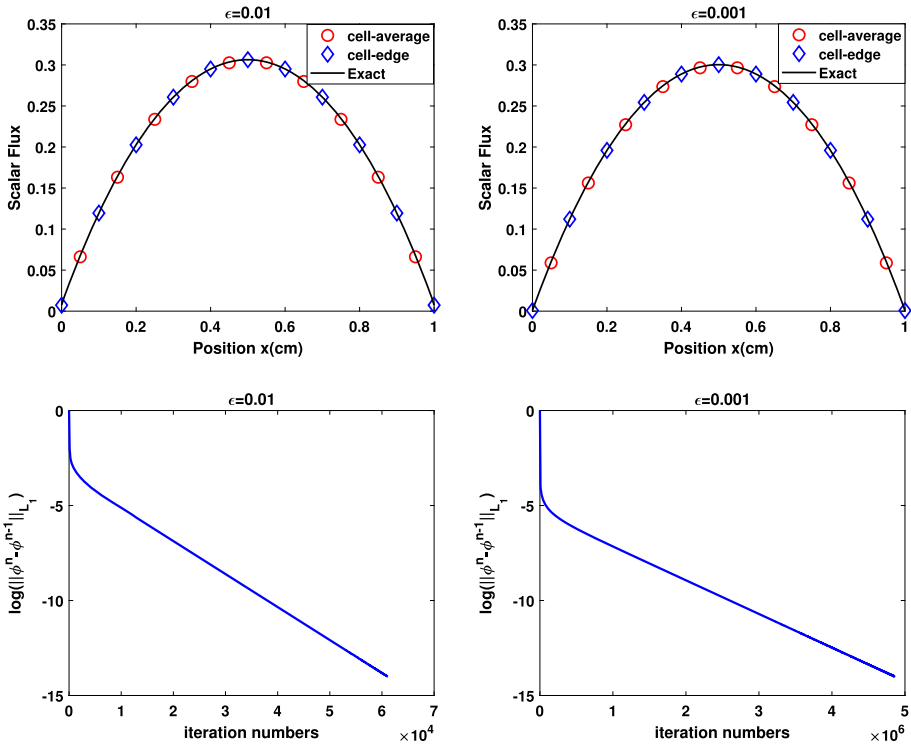


Fig. 4 Example 2 with $\Delta x = 0.1$. Numerical solutions (top); Iteration history (bottom); $\epsilon = 0.01$ (left); $\epsilon = 0.001$ (right)

4.2 One-Dimensional Problem with Anisotropic Incoming Flux

Example 3 This is also a 1D slab case, and the Gauss-Legendre S_{12} quadrature set is used for the angular discretization. The setup of the problem takes the form

$$L = 1, \quad \sigma_t = 1, \quad \sigma_a = 0.8, \quad Q = 1.$$

The incoming angular flux at $x = 0$ changes linearly from 0 to 5 for the six discrete incoming directions. On the right boundary at $x = 1$, the vacuum boundary is considered. Again, the analytical solution can be obtained following the approach discussed in [44]. Figure 5 shows the numerical solutions with spatial size $\Delta x = 0.1$ for different ϵ , which demonstrates that the HWENO FSM can capture the thick diffusion limit well in both the cell-average and cell-edge fluxes, for various values of ϵ . Furthermore, Table 2 lists the comparison of CPU times for the HWENO method with/without the hybrid strategy when $\epsilon = 0.001$, and we can observe a 50% saving in CPU times by the hybrid strategy.

4.3 One-Dimensional Problem with the Interior Thin Layer

Example 4 In this test, we consider a 1D slab consisting of two material regions. The left half of the slab is an optically thin region, and the right half is an optically thick diffusive region.

Table 5 Example 2.

$\varepsilon = 1, \text{FSM}$						$\varepsilon = 1, \text{GS iteration}$					
N	L_1 error	order	L_∞ error	iter	time	L_1 error	order	L_∞ error	iter	time	
10	1.80e-05	-	4.60e-05	109	0.005	1.80e-05	-	4.60e-05	166	0.009	
20	4.07e-07	5.47	2.19e-06	165	0.006	4.07e-07	5.47	2.19e-06	227	0.009	
40	5.50e-09	6.20	6.03e-08	275	0.009	5.50e-09	6.20	6.03e-08	308	0.018	
80	5.70e-11	6.59	1.25e-09	493	0.026	5.70e-11	6.59	1.25e-09	577	0.046	
160	6.85e-13	6.37	2.23e-11	920	0.087	7.13e-13	6.32	2.24e-11	1103	0.155	
$\varepsilon = 0.1, \text{FSM}$						$\varepsilon = 0.1, \text{GS iteration}$					
N	L_1 error	order	L_∞ error	iter	time	L_1 error	order	L_∞ error	iter	time	
10	2.18e-04	-	8.09e-04	2208	0.04	2.18e04	-	8.09e0-4	2308	0.08	
20	6.135e-05	1.82	3.46e-04	2628	0.06	6.13e-05	1.82	3.46e-04	2820	0.10	
40	8.90e-06	2.78	8.64e-05	3460	0.12	8.90e-06	2.78	8.64e-05	3836	0.22	
80	5.24e-07	4.08	9.11e-06	5100	0.34	5.24e-07	4.08	9.11e-06	5843	0.47	
160	1.39e-08	5.22	4.41e-07	8327	0.93	1.39e-08	5.22	4.41e-07	9793	1.29	
320	2.14e-10	6.02	1.27e-08	14654	2.82	2.14e-10	6.02	1.27e-08	17534	3.98	
$\varepsilon = 0.01, \text{FSM}$						$\varepsilon = 0.01, \text{GS iteration}$					
N	L_1 error	order	L_∞ error	iter	time	L_1 error	order	L_∞ error	iter	time	
10	4.62e-05	-	1.71e-04	27250	3	4.62e-05	-	1.71e-04	128020	3	
20	3.17e-05	0.54	1.78e-04	130430	4	3.17e-05	0.54	1.78e-04	131920	4	
40	1.89e-05	0.74	1.48e-04	136730	6	1.89e-05	0.74	1.48e-04	139630	8	
80	9.46e-06	1.00	9.08e-05	149200	9	9.46e-06	1.00	9.08e-05	154960	14	
160	3.57e-06	1.40	4.29e-05	173950	18	3.57e-06	1.40	4.29e-05	185330	27	
320	7.85e-07	2.18	1.33e-05	222820	44	7.80e-07	2.18	1.33e-05	245240	56	
640	7.26e-08	3.43	1.87e-06	319040	124	7.26e-08	3.43	1.87e-06	363080	161	
1280	2.71e-09	4.73	1.13e-07	507730	394	2.71e-09	4.74	1.13e-07	593920	521	

Comparison of the two iteration methods with $\omega = 0.5$: The errors of numerical solution, convergence rate and iteration numbers

Table 6 Example 2.

ϵ	L_1 error	order	L_∞ error	order
$N = 10$				
1	4.89e-01	–	5.05e-01	–
0.1	7.16e-02	0.83	7.98e-02	0.80
0.01	7.32e-03	0.99	8.19e-03	0.98
0.001	7.31e-04	1.00	8.11e-04	1.00
0.0001	7.31e-05	1.00	8.09e-05	1.00
$N = 20$				
1	4.89e-01	–	5.05e-01	–
0.1	7.20e-02	0.83	8.05e-02	0.79
0.01	7.38e-03	0.98	8.60e-03	0.97
0.001	7.37e-04	1.00	8.49e-04	1.00
0.0001	7.37e-05	1.00	8.46e-05	1.00

The errors and order of accuracy between numerical solution of S_N equation with different ϵ and the exact solution of the limit diffusion equation

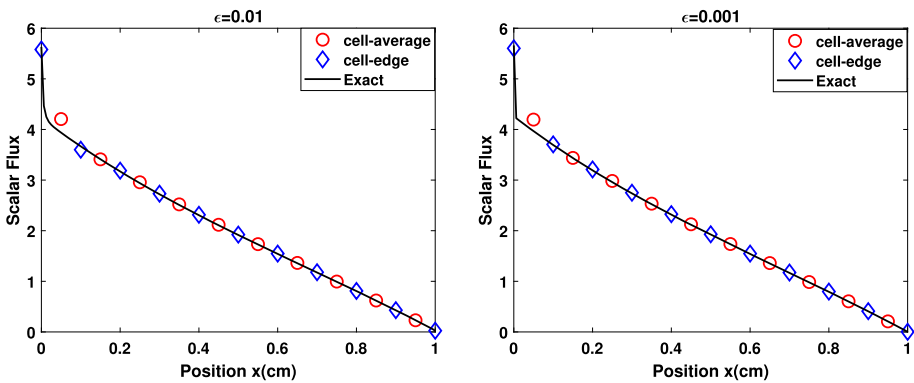


Fig. 5 Numerical solution of Example 3 with $\Delta x = 0.1$. $\epsilon = 0.01$ (left) and $\epsilon = 0.001$ (right)

The specifications of the problem are defined by $L = 2$,

$$\sigma_t = \begin{cases} \epsilon, & 0 \leq x < 1, \\ 1, & 1 \leq x < 2, \end{cases} \quad \sigma_a = \begin{cases} \frac{1}{\epsilon}, & 0 \leq x < 1, \\ 0.8, & 1 \leq x < 2, \end{cases} \quad \text{and} \quad Q = \begin{cases} 0, & 0 \leq x < 1, \\ 1, & 1 \leq x < 2. \end{cases}$$

Again, the Gauss-Legendre S_{12} quadrature set is used for the angular discretization. The incoming angular flux at $x = 0$ changes linearly from 0 to 5 for the six discrete incoming directions. On the right boundary at $x = 2$, the vacuum boundary is considered. The analytical solution of this problem in the form of cell-edge can be computed following the idea in [44]. Figure 6 shows the numerical solutions with spatial size $\Delta x = 0.2$ for different ϵ , which demonstrates that the HWENO FSM can capture the thick diffusion limit well in both the cell-average and cell-edge fluxes, for various values of ϵ .

For Examples 3 and 4, we also plotted the numerical results by the finite difference HWENO method in Fig. 7 for comparison. Again, it suggests that the finite difference method

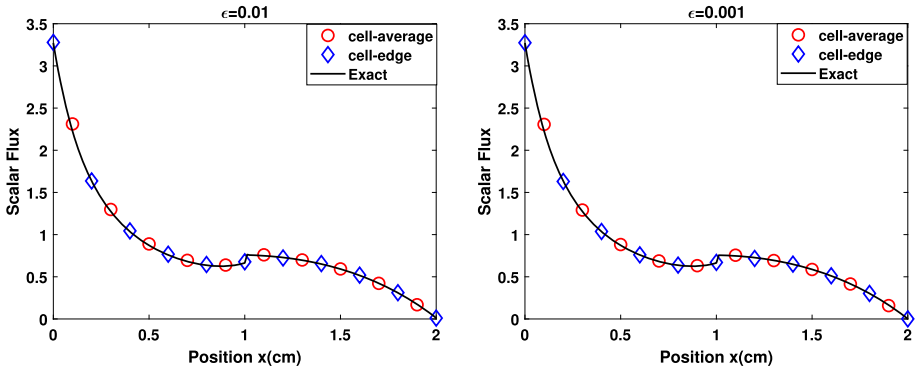


Fig. 6 Numerical solution of Example 4 with $\Delta x = 0.2$. $\varepsilon = 0.01$ (left) and $\varepsilon = 0.001$ (right)

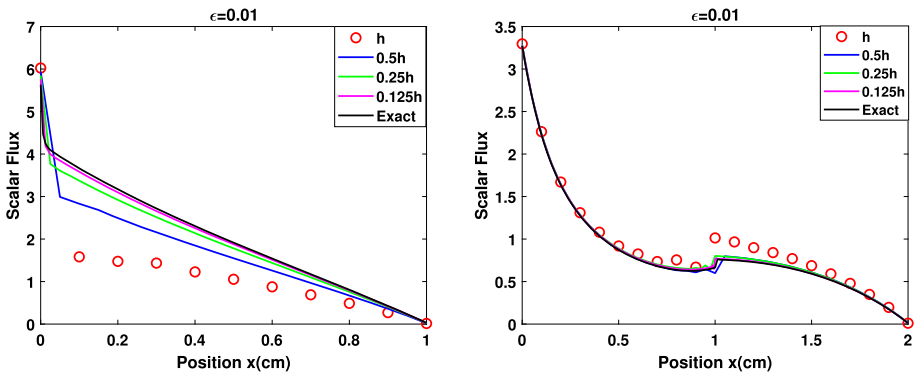


Fig. 7 Numerical solution of Example 3 and Example 4 through finite difference HWENO method. Example 3 with $h = \Delta x = 0.1$ (left) and Example 4 with $h = \Delta x = 0.1$ (right)

does not have the AP property, since the numerical solution does not overlap with the exact solution on the coarse mesh for small ε .

Remark 4.1 For the finite difference HWENO method, we performed some numerical examples, and observe numerically (Figs. 3 and 7) that it does not have the AP property. One possible reason is that, similar to other upwind finite difference schemes (for instance, step difference method), finite difference HWENO method is not an ε -uniform scheme, while finite volume HWENO method (which has some similarity with LD method or DG method which is automatically AP with at least linear elements) is. In general, upwind finite difference does not have the AP property [43].

Example 5 This is a classical example taking from [24]. We consider a slab in $[0, 11]$, $Q = 0$, $\varepsilon = 1$, and other settings are given by

$$\sigma_t = \begin{cases} 2, & 0 \leq x < 1, \\ 100, & 1 \leq x < 11, \end{cases} \quad \sigma_a = \begin{cases} 2, & 0 \leq x < 1, \\ 0, & 1 \leq x < 11, \end{cases} \quad \text{and} \quad \begin{cases} \psi(0, \mu) = 1, & \mu > 0, \\ \psi(11, \mu) = 0, & \mu < 0. \end{cases}$$

The problem consists of a two mean-free-path purely absorbing part and a 1000 mean-free-path purely scattering part. We solve this problem using the S_{12} quadrature set in the angular

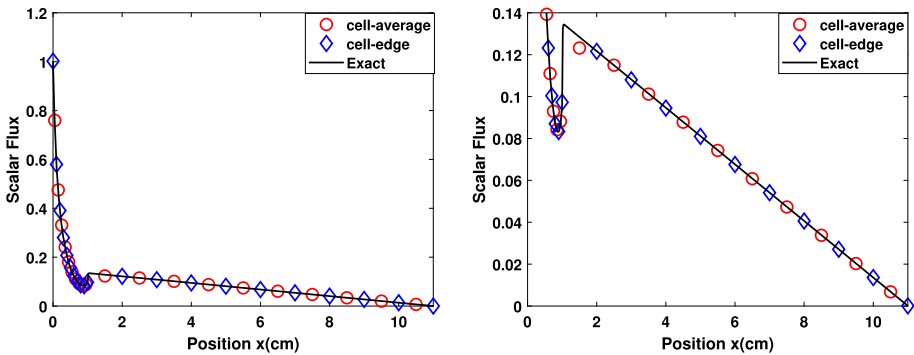


Fig. 8 Numerical solution of Example 5 on $N = 20$ (left). The zoomed-in version of Example 5 (right)

direction and the mesh size

$$\Delta x = \begin{cases} 0.1, & 0 \leq x < 1, \\ 1, & 1 \leq x < 11. \end{cases} \tag{4.1}$$

The “exact” cell-edge solution is obtained by LD method with a refined mesh of $N = 1000$. In the left plot of Fig. 8, we present the numerical results of HWENO method with the hybrid strategy, and the zoomed-in version is provided in the right plot of Fig. 8, which provides a better view of the numerical simulation near the interior layer. We can observe that the numerical solution is in good agreement with the exact solution, which indicates that the proposed HWENO method produces very accurate results for this challenging test.

Example 6 Another problem considered in [24] has the setup $L = 20$, $\varepsilon = 1$, $\sigma_t = 100$, and the other settings are given by

$$\sigma_a = \begin{cases} 10, & 0 \leq x < 10, \\ 0, & 10 \leq x < 20, \end{cases} \quad Q = \begin{cases} 10, & 0 \leq x < 10, \\ 0, & 10 \leq x < 20, \end{cases} \tag{4.2}$$

with vacuum boundary. The system in this problem consists of a 1000 mean free path slab, with absorption and a flat interior source, adjoining a 1000 mean free path purely scattering slab with no interior source. The “exact” cell-edge solution is obtained by the LD method with a refined mesh of $N = 100$. The Gauss-Legendre S_{12} quadrature set is used in the angular discretization. We take spatial size $\Delta x = 1$ and the numerical result of the HWENO method is provided in the Fig. 9, from which we can observe that the numerical solution is in good agreement with the exact solution.

For Examples 5 and 6, we also provided the CPU times comparison of the HWENO method with or without the hybrid strategy in Table 2, we can observe a 50% saving of CPU time when the hybrid strategy is used.

4.4 Two-Dimensional Problems

Only the cell-average fluxes will be plotted in the figures for the two-dimensional problems in this subsection.

Fig. 9 Example 6, Numerical solution of scalar fluxes with $\Delta x = 1$

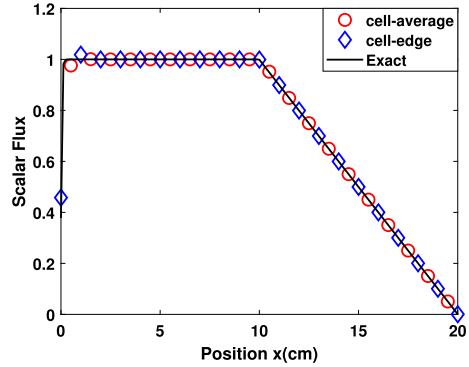


Table 7 Example 7.

N	L_1 error	order	L_∞ error	order	iter	time
$\varepsilon = 1$						
10	2.07e-03	–	1.05e-02	–	42	0.99
20	3.71e-05	5.80	3.70e-04	4.82	49	4.95
40	4.62e-07	6.32	8.73e-06	5.40	65	24.08
80	4.38e-09	6.72	1.56e-07	5.79	99	151.70
$\varepsilon = 0.1$						
10	7.93e-03	–	3.66e-02	–	1559	37.02
20	1.41e-04	5.80	1.40e-03	4.70	1621	146.84
40	2.04e-06	6.11	3.74e-05	5.22	1744	629.92
80	2.73e-08	6.22	8.43e-07	5.47	1990	1811.3

The errors, order of accuracy and CPU time of 2D HWENO method with hybrid strategy

Example 7 (Accuracy test with manufactured solution in 2D). To test the order of convergence of the 2D HWENO FSM, we follow the setup in [43] and consider the manufactured exact solution of the form

$$\psi(x, y, \mu_m, \eta_m) = x^3 y^3 (2 - x)^3 (2 - y)^3,$$

in the computational domain $\Omega = [0, 2] \times [0, 2]$. The other parameters are set as

$$\sigma_t = 1, \quad \sigma_a = 0.8,$$

and

$$Q(x, y) = \frac{4}{\varepsilon} [(24x^2 - 48x^3 + 30x^4 - 6x^5)y^3(2 - y)^3\mu_m + x^3(2 - x)^3(24y^2 - 48y^3 + 30y^4 - 6y^5)\eta_m] + 4\sigma_a\psi.$$

The numerical solutions are obtained using the level symmetric S_{12} quadrature set for angular discretization. We have run the simulations for $\varepsilon = 1$ and $\varepsilon = 0.1$. In Table 7, we show the numerical errors, iteration numbers, and the corresponding order of accuracy of the 2D HWENO method with the hybrid strategy, from which we can observe the expected high-order accuracy for both choices of ε . In Fig. 10, we plot the numerical solutions and iteration history with $\Delta x = \Delta y = 0.2$ and $\varepsilon = 1$ or $\varepsilon = 0.1$. In Fig. 11, we plot the numerical

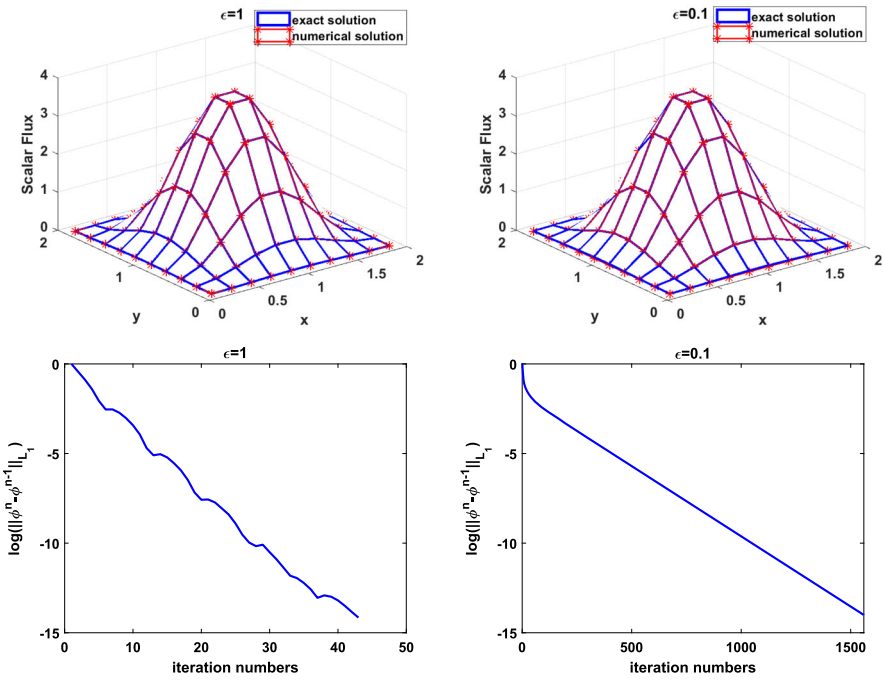


Fig. 10 Numerical solution of Example 7 with $\Delta x = \Delta y = 0.2$, and $\epsilon = 1$ (left) and $\epsilon = 0.1$ (right)

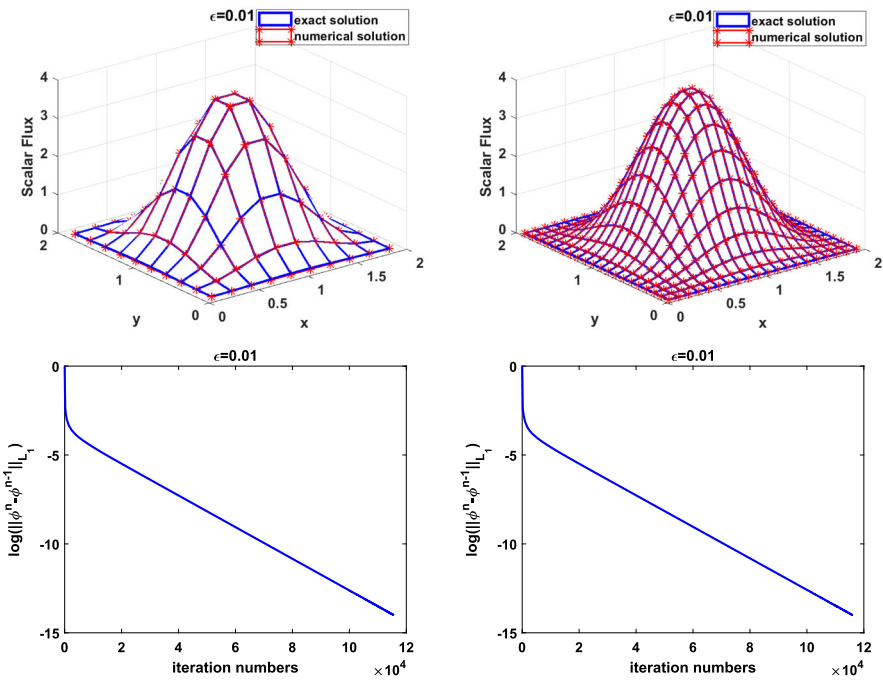


Fig. 11 Numerical solution of Example 7 with $\epsilon = 0.01$, and $\Delta x = \Delta y = 0.2$ (left) and $\Delta x = \Delta y = 0.1$ (right)

Table 8 Example 7.

$\varepsilon = 1$, FSM							$\varepsilon = 1$, GS iteration						
N	L_1 error	order	L_∞ error	order	iter	time	L_1 error	order	L_∞ error	order	iter	time	
10	2.19e-03	–	1.11e-02	–	102	1	2.19e-03	–	1.11e-02	–	114	1	
20	3.84e-05	5.83	3.87e-04	4.84	136	5	3.84e-05	5.83	3.87e-04	4.84	169	9	
40	4.74e-07	6.34	8.97e-06	5.43	208	45	4.74e-07	6.34	8.97e-06	5.43	302	65	
80	4.47e-09	6.72	1.59e-07	5.81	335	301	4.47e-09	6.72	1.59e-07	5.81	583	540	
$\varepsilon = 0.1$, FSM							$\varepsilon = 0.1$, GS iteration						
N	L_1 error	order	L_∞ error	order	iter	time	L_1 error	order	L_∞ error	order	iter	time	
10	7.97e-03	–	3.68e-02	–	2853	38	7.97e-03	–	3.68e-02	–	3116	51	
20	1.42e-04	5.80	1.41e-03	4.70	3192	178	1.42e-04	5.80	1.41e-03	4.70	3710	223	
40	2.08e-06	6.09	3.75e-05	5.23	3871	919	2.08e-06	6.09	3.75e-05	5.23	4896	1165	
80	2.79e-08	6.21	8.44e-07	5.47	5221	5014	2.79e-08	6.21	8.44e-07	5.47	7243	6825	

Comparison of the two iteration methods with $\omega = 0.5$: The errors of numerical solution, convergence rate and iteration numbers

solutions and iteration history with a smaller $\varepsilon = 0.01$ on two sets of computational meshes. From these figures, one could observe that the HWENO FSM can capture the thick diffusion limit well on coarse meshes.

In Table 8, we report the numerical results of FSM and the standard GS iteration, including numerical errors, convergence order, iteration numbers and CPU times. As in the 1D cases, we can observe the iteration numbers of FSM are smaller than those of GS iteration on the same meshes, and the FSM costs less CPU time with $\omega = 0.5$. In addition, the FSM can take a larger $\omega (= 0.85)$, which further reduces the computational time.

Example 8 In this example which was originally considered in [6], we study the problem on bounded domain with vacuum boundary conditions with the setup

$$\Omega = [0, 1]^2, \sigma_t = 1, \sigma_a = 1, \text{ and } Q = 1.$$

We take the spatial size $\Delta x = \Delta y = 0.05$ for this problem. Again, the level symmetric S_{12} quadrature set for angular discretization. The limit diffusion equation, when $\varepsilon \rightarrow 0$, is given by

$$\begin{cases} -\frac{1}{3}\Delta\psi(\mathbf{x}) + \psi(\mathbf{x}) = 1, & \mathbf{x} \in (0, 1)^2; \\ \psi(\mathbf{x}) = 0, & \mathbf{x} \in \partial(0, 1)^2, \end{cases} \tag{4.3}$$

and we plot its exact solution on the same spatial size in Fig. 12 as a reference solution.

In [6], it was shown that the two-dimensional LD method does not have the AP property and cannot capture the diffusion limit well. In Fig. 13, we plot the iteration history and numerical solutions of the 2D finite volume HWENO method for $\varepsilon = 0.1$ and $\varepsilon = 0.01$. The Fig. 14, we present the numerical solutions of the 2D finite volume HWENO method for different values of ε : 0.001 and 0.0001, we can observe that the diffusion limit is well captured by our method, which suggests that HWENO method has the designed AP property.

Example 9 The setup of the problem can be found in Fig. 15 with $\varepsilon = 1$, which consists of three subregions: the left part is a non-scattering region with no interior source, the middle

Fig. 12 Example 8: the reference exact solution of the limit diffusion equation

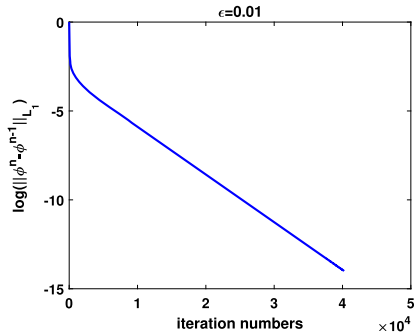
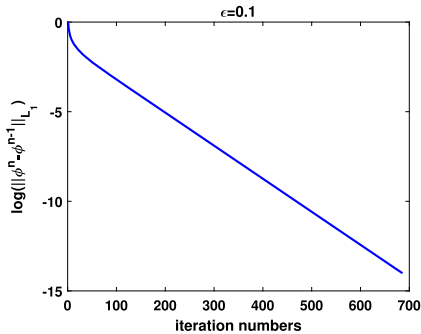
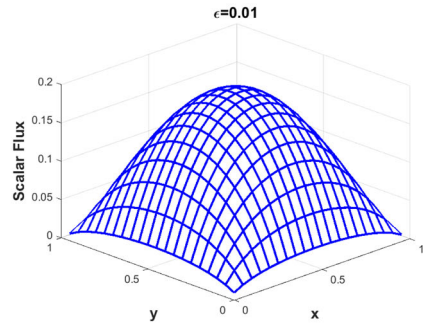
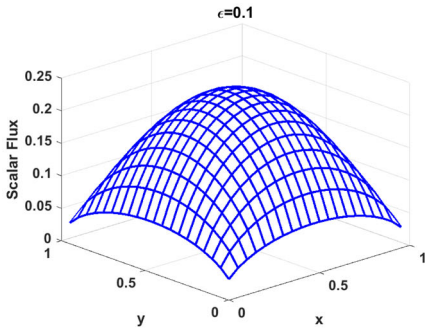
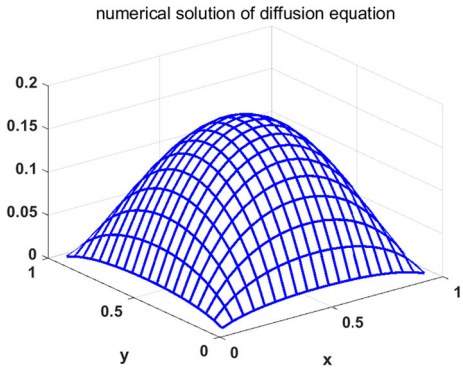


Fig. 13 Example 8, Numerical solution (top); iteration history (bottom); $\epsilon = 0.1$ (left); $\epsilon = 0.01$ (right)

part is an absorption region with an interior fixed source, and the right part is a high scattering region without interior source, and a natural vacuum boundary condition can be used for each side. The level symmetric S_{12} quadrature set is used for angular discretization. The numerical results of the proposed 2D HWENO method on different meshes are shown in Fig. 16, which again suggests that the finite volume HWENO FSM can capture the thick diffusion limit on coarse meshes.

Example 10 As discussed in [45], a potential issue with the diamond difference method and other high-order S_N numerical methods is that they could produce non-physical negative solutions when the domain contains large material inhomogeneity. In the last example, we

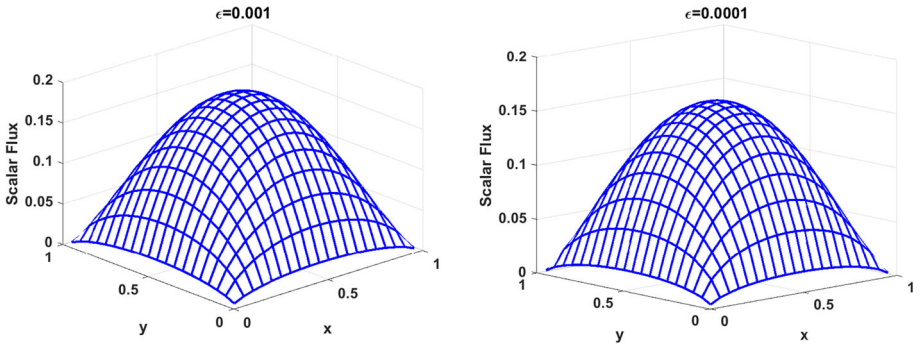


Fig. 14 Numerical solution of Example 8 with $\varepsilon = 0.001$ (left) and $\varepsilon = 0.0001$ (right)

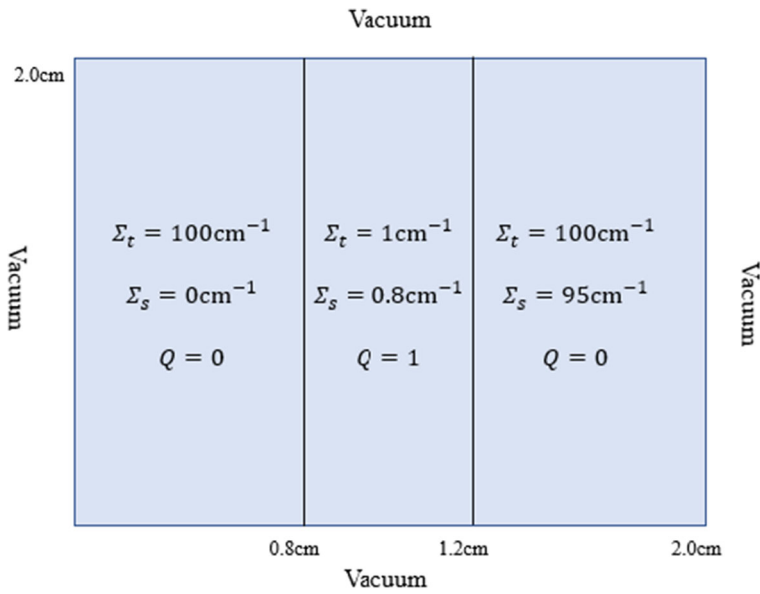


Fig. 15 Setup of Example 9, and $\sigma_t = \Sigma_t, \sigma_s = \Sigma_s$

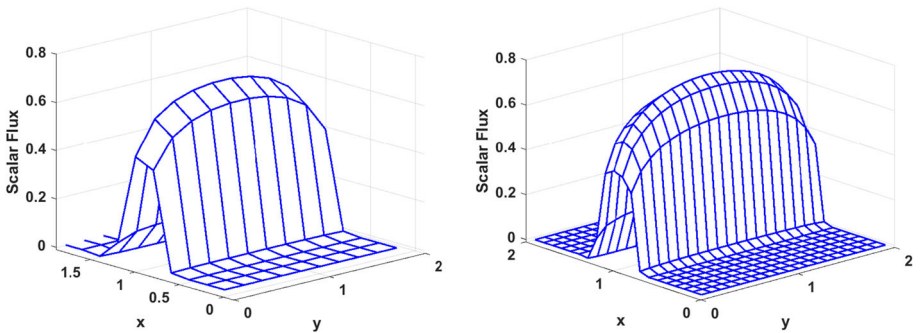
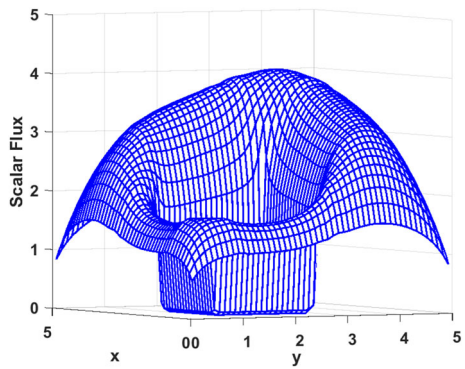


Fig. 16 Numerical solution of Example 9 with $\Delta x = \Delta y = 0.2$ (left) and $\Delta x = \Delta y = 0.1$ (right)

Fig. 17 Numerical solution of Example 10 with $\Delta x = \Delta y = 0.1$. Note that the numerical solutions stay positive and there is no negative or oscillatory solution



consider the following problem

$$\Omega = [0, 5]^2, \quad \sigma_t = \begin{cases} 1, & 0 \leq x < 1, \\ 100, & 1 \leq x < 3, \\ 1, & 3 \leq x \leq 5, \end{cases} \quad \sigma_a = \begin{cases} 0.05, & 0 \leq x < 1, \\ 95, & 1 \leq x < 3, \\ 0.05, & 3 \leq x \leq 5, \end{cases} \quad Q = 1 \quad (4.4)$$

and $\varepsilon = 1$. The vacuum boundary condition is considered. This problem is a 2D square problem and has a high absorbing region in the domain. The symmetric S_{12} quadrature is chosen for angular discretization. In Fig. 17, we plot the scalar flux distribution calculated by the proposed HWENO FSM under mesh size $\Delta x = \Delta y = 0.1$, from which we can observe the nice positivity-preserving property of the HWENO method for this example. We refer to [45, Fig 4] for the numerical result of diamond difference method, with negative values generated near the boundary of the absorbing region.

5 HWENO Fast Sweeping Method with DSA

In this section, we combine the proposed HWENO method proposed with the DSA method to verify that our method can be accelerated by DSA. The DSA method was first proposed by Kopp in [18] for the general transport equation, and Reed later showed that the numerical method was unstable for some problems with optical widths larger than one mean free path [38]. In [3], Alcouffe generalized it to the ordinate discrete transport equation, and designed DSA for the diamond difference method, and demonstrated for the first time that DSA could be used to significantly reduce the total CPU cost on practical problems. In [21] Larsen derived a DSA method for some difference schemes, and the spectral radius of the iterative method can be reduced by more than half. Adams et al. designed DSA for the DG method in [2]. Although the discretization of the transport equation and the diffusion equation is not strictly consistent, the accelerated scheme is unconditionally stable and the convergence is rapid.

The basic idea of the DSA method is to solve a diffusion equation of the form

$$-\frac{\partial}{\partial x} \left(\frac{1}{3\sigma_t} \frac{\partial}{\partial x} \delta\phi \right) + \sigma_a \delta\phi = \sigma_s [\phi], \quad (5.1)$$

with a given $[\phi]$, and then use the computed $\delta\phi$ to update the solution in order to yield a rapid convergence. In this paper, we take the S_N equation with a fixed-source as an example

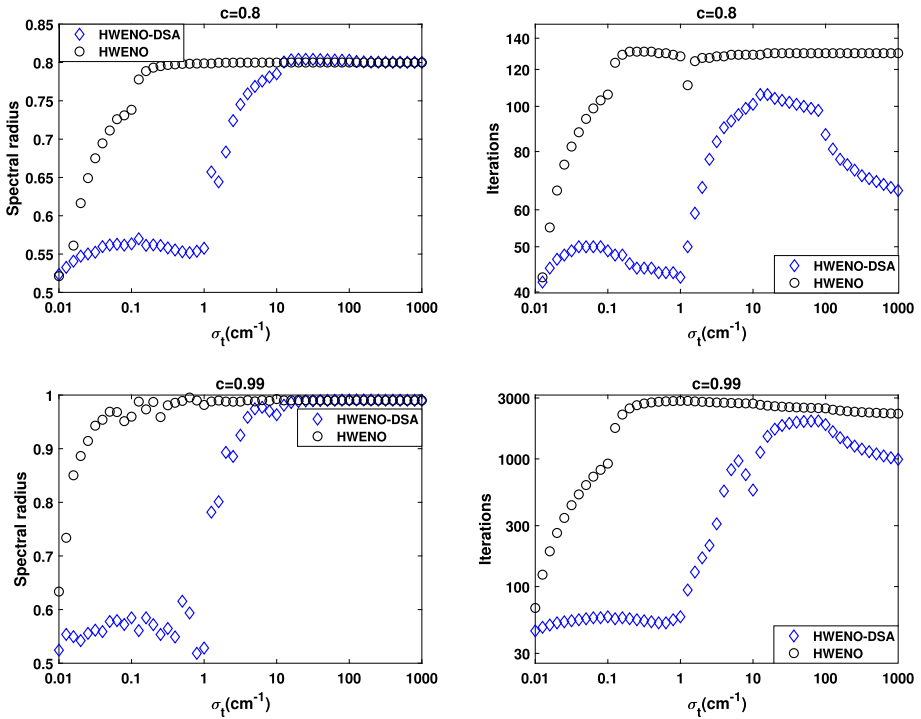


Fig. 18 Spectral radius (left) and iteration numbers (right), with a fifth-order extrapolation for ghost points. The y-axis of the right figure is on the log scale

to illustrate how HWENO method can be accelerated by the DSA algorithm. The general procedure is summarized as follows. Suppose $\tilde{\phi}^{n+1}$ to be the updated solution in each iteration of Algorithm 1. We set $\phi^{n+\frac{1}{2}} = \tilde{\phi}^{n+1}$, and solve the diffusion equation (5.1) for $\delta\phi$ with $[\phi] = \phi^{n+\frac{1}{2}} - \phi^n$. Then ϕ^{n+1} is updated by setting $\phi^{n+1} = \phi^{n+\frac{1}{2}} + \delta\phi$. More details about DSA can be found in [5].

One numerical example is provided to test the performance of HWENO method with DSA. We consider a fixed-source neutron transport equation as in [5], and a homogeneous 50-cm slab with the reflective right boundary and vacuum left boundary. The source term is $Q = 1$, and the spatial size is taken $\Delta x = 1$. The spectral radius of the convergence is calculated by

$$\rho = \frac{\|\phi^{n+1} - \phi^n\|}{\|\phi^n - \phi^{n-1}\|}.$$

For comparison, the spectral radius results of HWENO with DSA and without DSA are both studied, when two different scattering ratios $c = 0.8$ and $c = 0.99$ have been considered. In Fig. 18, the fifth-order extrapolation is used for ghost points, and we can observe that HWENO-DSA enjoys a smaller spectral radius when $\sigma_t < 10$. The spectral radius of the two methods is close to the theoretical value 0.8 and 0.99 if $\sigma_t > 10$, but it can be seen from the right plots of Fig. 18 that the iteration numbers of HWENO-DSA are still smaller than those of HWENO. In both cases, when $\sigma_t > 100$, the iteration numbers of HWENO-DSA will gradually decrease, but the iteration numbers of the HWENO method remain unchanged.

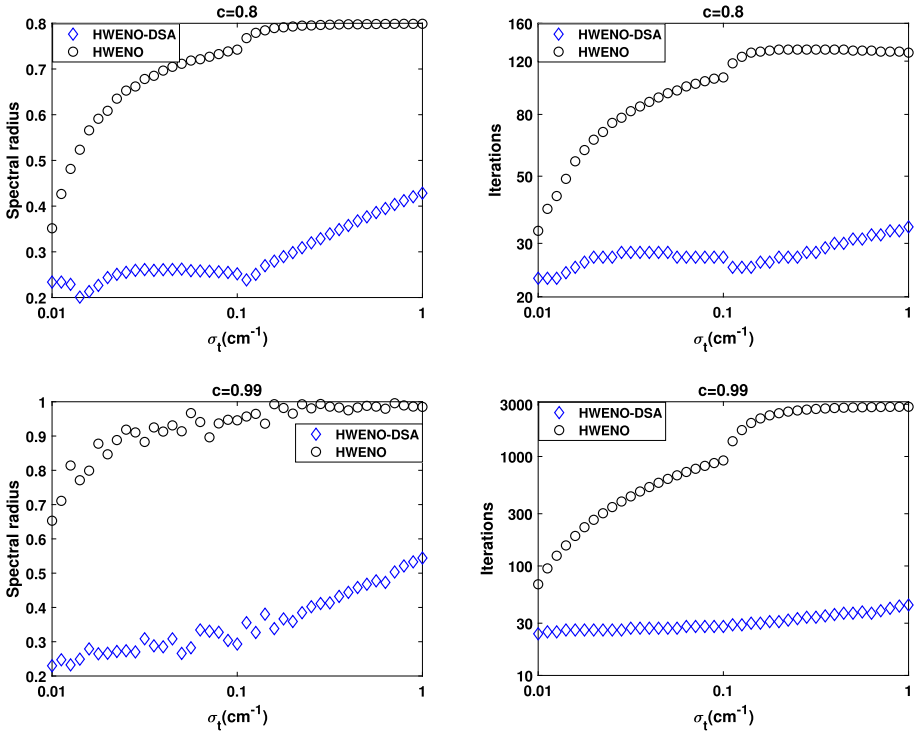


Fig. 19 Spectral radius and iteration numbers (right), with a second order extrapolation for ghost points. The y-axis of the right figure is on the log scale

If second-order extrapolations are used for the ghost points, as shown in Fig. 19, the spectral radius is close to 0.2 for the case of $\sigma_t < 0.1$, which is close to the theoretical value. Even if $0.1 < \sigma_t < 1$, it is still less than 0.5, which is acceptable for a high-order method.

6 Conclusion

In this paper, we combined the HWENO scheme and the fast sweeping method to numerically solve the steady-state S_N transport equations in the finite volume framework. The HWENO method is known to be more compact and produce smaller errors than the WENO method, and enjoys a simpler boundary treatment. The main contribution of this paper is to prove that the finite volume HWENO method preserves the asymptotic diffusion limit when ϵ goes to zero and has the asymptotic preserving property. One- and two-dimensional numerical examples show that HWENO FSM is of high-order accurate and can capture the thick diffusion limits on coarse meshes. We also combined the DSA algorithm with the HWENO method to accelerate the convergence. Numerical results show that the high-order HWENO method proposed in this paper can be accelerated with DSA, which makes the HWENO method more valuable in applications. The proposed method can be easily extended to any dimension on cartesian

meshes. The extension to unstructured meshes, as well as comparison with other high-order methods, will be discussed in future work.

Funding The work of Y. Xing is partially supported by the NSF grant DMS-1753581. The work of J. Qiu is partially supported by NSFC grant 12071392.

Data Availability All datasets generated during the current study are available from the corresponding author upon reasonable request.

Availability of data and material Available upon reasonable request.

Declarations

Conflict of interest The authors declare that they have no conflict of interest.

References

1. Adams, M.L.: Discontinuous Finite Element Transport Solutions in Thick Diffusive Problems. *Nucl. Sci. Eng.* **137**(3), 298–333 (2001)
2. Adams, M.L., Martin, W.R.: Diffusion synthetic acceleration of discontinuous finite element transport iterations. *Nucl. Sci. Eng.* **111**(2), 145–167 (1992)
3. Alcouffe, R.E.: Diffusion synthetic acceleration methods for the diamond-differenced discrete-ordinates equations. *Nucl. Sci. Eng.* **64**(2), 344–355 (1977)
4. Boué, M., Dupuis, P.: Markov chain approximations for deterministic control problems with affine dynamics and quadratic cost in the control. *SIAM J. Numer. Anal.* **36**(3), 667–695 (1999)
5. Byambaakhuu, T., Wang, D., Xiao, S.: A Coarse-Mesh Diffusion Synthetic Acceleration Method with Local hp Adaptation for Neutron Transport Calculations. *Nucl. Sci. Eng.* **192**(2), 208–217 (2018)
6. Börgers, C., Larsen, E.W., Adams, M.L.: The asymptotic diffusion limit of a linear discontinuous discretization of a two-dimensional linear transport equation. *J. Comput. Phys.* **98**(2), 285–300 (1992)
7. Chen, S.: Fixed-point fast sweeping WENO methods for steady-state solution of scalar hyperbolic conservation laws. *Int. J. Numer. Anal. Model* **11**(1), 117–130 (2014)
8. Chen, W., Chou, C.-S., Kao, C.-Y.: Lax-Friedrichs fast sweeping methods for steady-state problems for hyperbolic conservation laws. *J. Comput. Phys.* **234**, 452–471 (2013)
9. Carlson, B.G., Lathrop, K.D.: *Computing methods in reactor physics*. Gordon and Breach, New York (1968)
10. Castor, J.I.: Comparison of the Errors of the Wilson and Feautrier Schemes for Differencing the Equation of Transfer as Applied to a Class of Simple Model Problems. Lawrence Livermore National Laboratory memorandum (Jan. 29, 1982) and addendum (Feb. 2, 1982), (1982)
11. Godunov, S., Bohachevsky, I.: Finite difference methods for the computation of discontinuous solutions of the equations of fluid dynamics. *Math. Sbornik* **47**(3), 271–306 (1959)
12. Guermont, J.L., Kanschat, G.: Asymptotic analysis of upwind discontinuous Galerkin approximation of the radiative transport equation in the diffusive limit. *SIAM J. Numer. Anal.* **48**(1), 53–78 (2010)
13. Habetler, G.J., Matkowsky, B.J.: Uniform asymptotic expansions in transport theory with small mean free paths, and the diffusion approximation. *J. Math. Phys.* **16**(4), 846–854 (1975)
14. Huang, L., Shu, C.-W., Zhang, M.P.: Numerical boundary conditions for the fast sweeping high order WENO methods for solving the Eikonal equation. *J. Comput. Math.* **26**(3), 336–346 (2008)
15. Jiang, G., Shu, C.-W.: Efficient implementation of weighted ENO schemes. *J. Comput. Phys.* **126**(1), 202–228 (1996)
16. Jin, S.: Efficient asymptotic-preserving (ap) schemes for some multiscale kinetic equations. *SIAM J. Sci. Comput.* **21**, 441–454 (1999)
17. Kao, C.-Y., Osher, S., Qian, J.: Lax-Friedrichs sweeping scheme for static Hamilton-Jacobi equations. *J. Comput. Phys.* **196**(1), 367–391 (2004)
18. Kopp, H.J.: Synthetic Method Solution of the Transport Equation. *Nucl. Sci. Eng.* **17**(1), 65–74 (1963)
19. Larsen, E.W.: Diffusion theory as an asymptotic limit of transport theory for nearly critical systems with small mean free paths. *Ann. Nucl. Energy* **7**(4–5), 249–255 (1980)
20. Larsen, E.W.: The asymptotic diffusion limit of discretized transport problems. *Nucl. Sci. Eng.* **112**(4), 336–346 (1992)

21. Larsen, E.W.: Unconditionally stable diffusion-synthetic acceleration methods for the slab geometry discrete ordinates equations, Part I: Theory. *Nucl. Sci. Eng.* **82**(1), 47–63 (1982)
22. Larsen, E.W., Keller, J.B.: Asymptotic solution of neutron transport problems for small mean free paths. *J. Math. Phys.* **15**(1), 75–81 (1974)
23. Larsen, E.W., Morel, J.E.: *Advances in discrete-ordinates methodology*. Nuclear Computational Science, Springer, pp. 1–84 (2010)
24. Larsen, E.W., Morel, J.E.: Asymptotic Solutions of Numerical Transport Problems in Optically Thick, Diffusive Regimes II. *J. Comput. Phys.* **83**, 212–236 (1989)
25. Larsen, E.W., Morel, J.E., Miller, W.F., Jr.: Asymptotic Solutions of Numerical Transport Problems in Optically Thick, Diffusive Regimes. *J. Comput. Phys.* **69**(2), 283–324 (1987)
26. Larsen, E.W., Pomraning, G.C., Badham, V.C.: Asymptotic analysis of radiative transfer problems. *J. Quant. Spectrosc. Radiat. Transf.* **29**(4), 285–310 (1983)
27. Li, F., Shu, C.-W., Zhang, Y.-T., Zhao, H.: Second order discontinuous Galerkin fast sweeping method for Eikonal equations. *J. Comput. Phys.* **227**(17), 8191–8208 (2008)
28. Liu, H., Qiu, J.: Finite Difference Hermite WENO schemes for conservation laws. *J. Sci. Comput.* **63**, 548–572 (2015)
29. Lund, C.M.: *Radiation Transport in Numerical Astrophysics*. nuas, 498, (1985)
30. Lund, C.M., Wilson, J.R.: Some numerical methods for time-dependent multifrequency radiation transport calculations in one dimension. UCRL-84678, Lawrence Livermore National Laboratory, Livermore, CA, (1980)
31. Luo, S.: A uniformly second order fast sweeping method for Eikonal equations. *J. Comput. Phys.* **241**(10), 104–117 (2013)
32. Papanicolaou, G.C.: Asymptotic analysis of transport processes. *Bull. New. Ser. Am. Math. Soc.* **81**(2), 330–392 (1975)
33. Pitkäranta, J.: On the spatial differencing of the discrete ordinate neutron transport equation. *SIAM J. Numer. Anal.* **15**(5), 859–869 (1978)
34. Qian, J., Zhang, Y.-T., Zhao, H.-K.: A fast sweeping method for static convex Hamilton-Jacobi equations. *J. Sci. Comput.* **31**(1), 237–271 (2007)
35. Qiu, J., Shu, C.-W.: Hermite WENO schemes and their application as limiters for Runge-Kutta discontinuous Galerkin method: one dimensional case. *J. Comput. Phys.* **193**(1), 115–135 (2004)
36. Qiu, J., Shu, C.-W.: Hermite WENO schemes and their application as limiters for Runge-Kutta discontinuous Galerkin method II: two-dimensional case. *Comput. Fluids* **34**(6), 642–663 (2005)
37. Qiu, J., Shu, C.-W.: Hermite WENO schemes for Hamilton-Jacobi equations. *J. Comput. Phys.* **204**(1), 82–99 (2005)
38. Reed, W.H.: The effectiveness of acceleration techniques for iterative methods in transport theory. *Nucl. Sci. Eng.* **45**(3), 45–254 (1971)
39. Ren, Y., Xing, Y., Qiu, J.: High order finite difference Hermite WENO fast sweeping methods for static Hamilton-Jacobi equations. *J. Comput. Math.*, In press
40. Ren, Y., Xing, Y., Qiu, J.: High order finite difference Hermite WENO fixed-point fast sweeping method for static Hamilton-Jacobi equations. *Commun. Comput. Phys.* **31**, 154–187 (2022)
41. Tsai, R., Cheng, L.T., Osher, S., Zhao, H.-K.: Fast sweeping algorithms for a class of Hamilton-Jacobi equations. *SIAM J. Numer. Anal.* **41**(2), 673–694 (2003)
42. Wang, D.: On a Recent Theoretical Result on Diffusion Limits of Numerical Methods for the SN Transport Equation in Optically Thick Diffusive Regimes, The 26th International Conference on Transport Theory (ICTT-26) Sorbonne University, Paris, France, September, 23-27 (2019)
43. Wang, D.: The Asymptotic Diffusion Limit of Numerical Schemes for the S_N Transport Equation. *Nucl. Sci. Eng.* **193**(12), 1339–1354 (2019)
44. Wang, D., Byambaakhuu, T.: A New Analytical S_N Solution in Slab Geometry. *Trans. Am. Nucl. Soc.* **117**(1), 757–760 (2017)
45. Wang, D., Byambaakhuu, T.: High Order Lax-Friedrichs WENO Fast Sweeping Methods for the S_N Neutron Transport Equation. *Nucl. Sci. Eng.* **193**(9), 982–990 (2019)
46. Wu, L., Zhang, Y.-T.: A third order fast sweeping method with linear computational complexity for Eikonal equations. *J. Sci. Comput.* **62**(1), 198–229 (2015)
47. Wu, L., Zhang, Y.-T., Zhang, S., Shu, C.-W.: High order fixed-point sweeping WENO methods for steady-state of hyperbolic conservation laws and its convergence study. *Commun. Comput. Phys.* **20**(4), 835–869 (2016)
48. Xiong, T., Zhang, M.P., Zhang, Y.-T., Shu, C.-W.: Fast sweeping fifth order WENO scheme for static Hamilton-Jacobi equations with accurate boundary treatment. *J. Sci. Comput.* **45**(1–3), 514–536 (2010)
49. Zhang, Y.-T., Chen, S., Li, F., Zhao, H.-K., Shu, C.-W.: Uniformly accurate discontinuous Galerkin fast sweeping methods for Eikonal equations. *SIAM J. Sci. Comput.* **33**(4), 1873–1896 (2011)

50. Zhang, Y.-T., Zhao, H.-K., Chen, S.: Fixed-point iterative sweeping methods for static Hamilton-Jacobi equations. *Methods Appl. Anal.* **13**(3), 299–320 (2006)
51. Zhang, Y.-T., Zhao, H.-K., Qian, J.: High Order fast sweeping methods for static Hamilton-Jacobi equations. *J. Sci. Comput.* **29**(1), 25–56 (2006)
52. Zhao, H.-K.: A fast sweeping method for Eikonal equations. *Math. Comput.* **74**(250), 603–627 (2005)
53. Zhao, Z., Qiu, J.: A Hermite WENO scheme with artificial linear weights for hyperbolic conservation laws. *J. Comput. Phys.* **417**, 109583 (2020)
54. Zheng, F., Qiu, J.: Directly solving the Hamilton-Jacobi equations by Hermite WENO Schemes. *J. Comput. Phys.* **307**, 423–445 (2016)

Publisher's Note Springer Nature remains neutral with regard to jurisdictional claims in published maps and institutional affiliations.

Springer Nature or its licensor holds exclusive rights to this article under a publishing agreement with the author(s) or other rightsholder(s); author self-archiving of the accepted manuscript version of this article is solely governed by the terms of such publishing agreement and applicable law.

Authors and Affiliations

Yupeng Ren^{1,2} · Yulong Xing³  · Dean Wang⁴ · Jianxian Qiu⁵

Yupeng Ren
ypren@stu.xmu.edu.cn

Dean Wang
wang.12239@osu.edu

Jianxian Qiu
jxqiu@xmu.edu.cn

¹ Beijing Computational Science Research Center, Beijing 100193, People's Republic of China

² School of Mathematical Sciences, Xiamen University, Xiamen, Fujian 361005, People's Republic of China

³ Department of Mathematics, The Ohio State University, Columbus, OH 43210, USA

⁴ Department of Mechanical and Aerospace Engineering, The Ohio State University, Columbus, OH 43210, USA

⁵ School of Mathematical Sciences and Fujian Provincial Key Laboratory of Mathematical Modeling and High-Performance Scientific Computing, Xiamen University, Xiamen, Fujian 361005, People's Republic of China